The ECPC Coupled Prediction Model

E. Yulaeva, M. Kanamitsu, and J. Roads

Experimental Climate Prediction Center
Climate Research Division
Scripps Institution of Oceanography, UCSD

First submitted to Monthly Weather Review June 27, 2006

Corresponding author address:
Dr. Elena Yulaeva, Experimental Climate Prediction Center
Climate Research Division, Scripps Institution of Oceanography
UCSD, 0224, La Jolla, CA 92093-0224,
e-mail: eyulaeva@ucsd.edu

Abstract.

This paper presents the new Experimental Climate Prediction Center (ECPC) Coupled Prediction Model (ECPM). The ECPM includes the Jet Propulsion Laboratory (JPL) version of the Massachusetts Institute of Technology (MIT) ocean model coupled to the ECPC version of the National Centers for Environmental Research (NCEP) Atmospheric Global Spectral Model (GSM). The adjoint and forward versions of the MIT model forced with the NCEP atmospheric analyses are routinely used at JPL for ocean state assimilation. An earlier version of the GSM was used for the NCEP/DOE Reanalysis-2 project and for operational seasonal forecasts at NCEP.

The ECPM climatology and internal variability derived from a 56-year long coupled integration are compared to the observations and reanalysis data. Though the ECPM exhibits climatological biases, these biases are relatively small and comparable to the systematic errors produced by other well known coupled models, including the recent NCEP Climate Forecast System (CFS).

The internal variability of the model, especially the tropical variability, resembles observations. The spectra of the simulated sea surface temperature, averaged over Nino3.4 region, exhibits maxima at frequencies corresponding to 3-6 year periods, indicating that the model simulates ENSO variability reasonably well. The model also produces 500-hPa height responses to tropical variability that are quantitatively similar to the observations

The skill of the ECPM in predicting 1994- 2006 SST anomalies over the NINO3.4 region is shown to be comparable to other coupled models. These retrospective forecasts were used for deriving a model climatology for real time seasonal forecasts that are currently produced and displayed at ECPC.

1. Introduction

Dynamical seasonal forecasts with time scales ranging from a few months to a year are now commonly performed at operational weather centers around the world. Although the accuracy of the forecasts are still marginal in comparison to statistical methods (Oldenborgh et al. 2005; Saha et al. 2006) continued efforts to improve the numerical modeling systems should eventually provide dynamical seasonal forecast products as useful as current dynamical forecasts for short and medium range predictions. In addition, unlike statistical methods, a dynamical forecast model is capable of providing other valuable data which can be used to understand the evolution of the atmosphere and ocean, and can thus further improve future seasonal prediction itself.

There are currently two kinds of dynamical seasonal forecasting methodologies. One forces an atmospheric model with independently predicted sea surface temperature anomalies (SSTAs). Predicted SSTAs are produced either by purely statistical methods (i.e. persisted anomalies) or by combined statistical and ocean-atmosphere coupled system forecasts. This method is called a "two-tier" forecast, and is used widely, since it is easier to implement and simpler to make reasonable forecast (see for example, Roads et al. 2001; Kanamitsu et al. 2002; Straus et al. 2003). The weakness of this method is that the atmospheric model is forced by SST but the ocean is not subsequently affected by the atmosphere. In the real world, the SST is determined by the mutual interaction between the ocean and atmosphere, and the "two-tier" models' lack of interaction may result in unphysical behaviors. For example, in regions where SST anomalies are driven by the atmosphere (like the central North Pacific and tropical monsoon regions) there could be huge discrepancies between simulated and observed direction of the air-sea flux exchange in two-tier system. As was shown in Wu et al. (2005), the inclusion of coupling increases the skill of the simulation of the air-sea interaction, which then leads to a

better prediction of monsoon activity

The second method is to use a dynamically coupled ocean-atmosphere system, the "one-tier" forecast. Initially a statistical or empirical correction (flux adjustment) was frequently used at the interface between the ocean and atmospheric models but recent improvements in both atmospheric and ocean models have now made it possible to avoid such corrections. Some form of statistical correction may still be needed for the final model output, but the forecast system itself is free from statistical corrections and thus the state of the ocean, including SST, and the atmosphere are dynamically and physically consistent and not overly artificially constrained.

The factors that greatly influence the skill of the seasonal forecast (in addition to the accuracy of the atmospheric and ocean models, and their coupling method) are the initial conditions. For an atmospheric forecast, the initial conditions are not crucial for time leads beyond about a month, since long-term forecasts are boundary forcing problems (e. g. Reichler and Roads 2003). However, certain atmospheric initial conditions, including those associated with anomalous stratosphere states, may still be important (Baldwin and Dunkerton 1999; Reichler and Roads 2004, 2005a,b). Oceanic initial conditions are certainly critical, since the seasonal ocean forecast is an initial value problem. In fact, in some cases ocean forecasts out to at least a year are strongly dependent on how accurate the ocean initial conditions were. In addition, the ocean initial conditions need to be "balanced" with the ocean and atmospheric models, otherwise, the integration goes through an initial adjustment, which contaminates the initial ocean condition and makes it difficult to use the forecast during the adjustment period. This adjustment period frequently exceeds several months, nearly the entire duration of the seasonal forecast (e. g. Rosati et al, 1997). In this regard, a data assimilation system for the ocean is critical for a coupled model seasonal forecast; just like atmospheric data assimilation is

essential for short and medium range atmospheric forecasts. There are additional requirements for land and ocean sea ice initial conditions, but we will not delve into this further since our focus here is on ocean atmosphere interactions.

When we actually perform a real time coupled forecast, the requirement of accurate ocean initial conditions places severe limits on the choice of ocean model, since the ocean model needs to have its own data assimilation and in addition, the ocean analysis system needs to be running in near real time. Variational data assimilation usually involves developing an adjoint of the ocean model, which requires considerable expertise and time to develop. The most widely used ocean model with a data assimilation component is the Geophysical Fluid Dynamics Laboratory (GFDL) Modular Ocean Model (MOM, see Derber and Rosati 1989; Carton et al. 2000,). This ocean data assimilation has now been running in real time at NCEP (Ji et al. 1995; Ji et al. 1998) for more than 10 years. MOM is very portable and easy to adopt, thus, most coupled models developed and used in U.S. utilize the GFDL ocean model, with a wide variety of atmospheric models coupled to it. Unfortunately, this current limited ocean analysis and model choice may severely limit the true scope of multi-model ensemble coupled model forecasts. At least the coupled forecast system at NASA/Global Modeling and Assimilation Office (GMAO), developed by Schopf and Loughe (1995), does provide an independent ocean model and analysis.

In this paper, we present a new seasonal forecast system, which utilizes an ocean model developed independently from GFDL and NASA/GMAO, coupled to our version of the NCEP seasonal forecast model. The oceanic component of this forecast system is the MIT model that comes with an advanced 4-D variational data assimilation system. Though the MIT GCM was primarily developed for research, ocean assimilation has been run quasi-operationally at JPL for the last several years. We will demonstrate that our new 1-tier Experimental Climate Prediction

Center (ECPC) Coupled Prediction Model (ECPM), without flux adjustment, produces skillful seasonal forecasts, which are comparable to other coupled forecast systems.

One rather important component of the seasonal forecast, missing in this study, needs to be mentioned here. A seasonal forecast is itself probabilistic in nature, particularly the atmospheric part, but also the coupled ocean component. The natural variability that is essentially noise in the forecast has to be filtered out by computing ensemble averages. A probability density function can also be obtained from ensemble forecasting, although its usage is still limited. Unfortunately, we did not have sufficient computer resources to perform large ensemble predictions in this initial study. All the forecasts presented here consist of a single member deterministic forecast. Therefore, we concentrate here on the average error components of atmosphere and ocean on broad scales (e. g. Moore and Kleeman, 1996).

This paper is structured as follows. After first describing the coupled modeling system in Section 2, we will describe the main features of a long continuous coupled model integration starting with consistent oceanic and atmospheric conditions in Section 3. We then present many coupled model retrospective forecasts starting at different months in Section 4. We will then examine how the skill of the seasonal forecast depends on the initial conditions and forecast lead-time in Section 5. In the same section we will study the importance of the coupling for improving the skill of long lead climate prediction by comparing coupled and uncoupled runs. Section 6 concludes the paper.

2. Models and Experiments

ECPM consists of the ECPC version of the NCEP Global Spectral Model (GSM) and the JPL version of the MIT ocean model that has been used for an ocean analysis each month beginning in 1993. The coupling is performed every 24 hours. The atmospheric model net heat,

fresh water, short and long wave radiation fluxes together with wind stresses are passed to the ocean component, while the atmosphere is forced with the SSTs obtained from the oceanic module. No flux adjustment is used in the coupled system. A difference between the ECPC coupling procedure and the one utilized in the NCEP CFS is that the numerical interaction between the atmosphere and ocean is global, and not confined to climatology at higher latitudes. The only climatology that is currently used in the model is the sea ice extent. We are planning to eventually include the correct description of the internal ice dynamics that will then allow for more realistic heat and fresh water transports and better calculation of air-sea fluxes at high latitudes. Further details about the models are provided below.

2.1 MIT OGCM

The oceanic component of the ECPM is the JPL MIT model, which has 1°x1° horizontal resolution with a telescoping (1/3°) resolution near the equator. The ocean model also has fine vertical resolution with 46 vertical levels. The vertical depth goes down to 5800 m, with the first 23 levels located in the upper 400 meters. The model is based on the primitive equations on a sphere under the Boussinesq approximation. There are prognostic equations for horizontal velocity, heat and salt, which are integrated forward in time on a staggered grid. At each time step the internal pressure is calculated from the hydrostatic relation, and the vertical velocity is diagnosed from the continuity equation. Spatial coordinates are longitude, latitude, and height. A detailed description of the model is provided in Marshall et al. (1997a, 1997b). We are using the version of the model with an implicit free surface. A full surface non-local K-Profile Parameterization (KPP) of vertical mixing throughout a water column is also used, and is described in detail in Large et al. (1994). The KPP model of vertical mixing parameterization is based on parameters derived from observational data; thus it captures important physics during

the annual cycle for a wide range of dynamical regimes and at the same time does not significantly increase computational time. A convective adjustment is used to remove gravitational instabilities underneath the surface mixed layer.

Finite volume techniques are employed yielding an intuitive discretization and support for the treatment of irregular geometries with orthogonal curvilinear grids. The algorithm can conveniently exploit massively parallel computers and has a domain decomposition, which allocates vertical columns of ocean to each processing unit. The model can arbitrarily handle complex geometry and is efficient and scalable. A ``pressure correction" method is used which is solved as a Poisson equation for the pressure field with Neumann boundary conditions in a geometry as complicated as that of the ocean basins. The pressure field is separated into surface, hydrostatic, and non-hydrostatic components. A preconditioned conjugate-gradient iteration is used to invert symmetric elliptic operators in both two and three dimensions. Physically motivated pre-conditioners are designed, which are efficient at reducing computation and minimizing communication between processors.

The assimilation (Kalman filter with Green's function tuned parameters) and forward simulation versions of the MIT model forced with NCEP reanalysis data are routinely used at JPL for ocean state assimilation (Fukumori 2002). In order to produce a computationally efficient data assimilation, JPL adopted a hierarchal assimilation system. First, a series of Green’s function are calculated and used for the correction of robust biases in the mean state; second a Kalman filter and smoother produces near real-time analysis of the time-dependent state. The system assimilates observed sea level and temperature profiles. Near real-time analyses are available at the JPL data server (http://ecco.jpl.nasa.gov/external) as ten-day averages.

The ocean analysis has been used in numerous studies of ocean variability as well as in various geodetic studies. These studies have demonstrated the accuracy of the JPL data assimilation system (see for instance Dickey et al. 2002; Stammer et al. 2002) and its applicability for a wide range of climate variability studies.

2.2 Global Spectral Model

The atmospheric component of the ECPM is the ECPC version of the NCEP GSM (Kanamitsu et al. 2003). An earlier version of the GSM is being used for operational seasonal forecast at NCEP and its performance was documented in Kanamitsu et al. (2003). (An upgraded version of the model is used as the atmospheric component in the current NCEP CFS.) Two-tier ensemble forecasts of the ECPC GSM are routinely being provided to the International Research Institute (IRI) as part of their multi-model seasonal forecast ensemble. Robertson et al. (2004) showed that the addition of these two-tier ECPC forecasts increased the IRI multi-model forecast skill, especially over Africa.

The GSM utilizes spherical harmonics as the basis functions and has an efficient transformation to a Gaussian grid for calculation of nonlinear terms and physics. Horizontal resolution is T62 (~200 Km) but the number of grid points is reduced in higher latitudes to save computer time (Juang, 2004). There are 28 vertical sigma (Phillips 1959) coordinate levels. The vertical domain is from the earth's surface (sigma=1) to the top of the atmosphere (sigma=0). This domain is divided into 28 layers with enhanced resolution near the bottom and the top of the model. Global and regional versions of the model are also used for experimental sub-seasonal to seasonal climate predictions at ECPC (see Roads, 2004). The main time integration scheme is leapfrog scheme for nonlinear advection terms, and semi-implicit scheme for gravity waves. An Asselin (1972) time filter is used to reduce computational modes.

Atmospheric model dynamics are based on the conservation of mass, momentum, energy and moisture. In order to take advantage of the spectral technique in the horizontal, the momentum equation is replaced by the vorticity and divergence equations (Bourke, 1974). Thus the model is basically described as a set of primitive equations with vorticity, divergence, logarithm of surface pressure, specific humidity and virtual temperature as dependent variables. Scale-selective, second-order horizontal diffusion (Leith, 1971) is applied to vorticity, divergence, and virtual temperature. The diffusion of temperature is performed on quasi-constant pressure surfaces (Kanamitsu et al. 1991). Implicit integration with a special time filter (Kalnay and Kanamitsu, 1988) is used for vertical diffusion. In order to incorporate physical tendencies into the semi-implicit integration scheme, a special adjustment scheme is performed (Kanamitsu et al., 1991).

The physics are written in the form of an adjustment and executed in sequence. The physical processes parameterizations originated from NCEP-DOE reanalysis (R-2) (see Kanamitsu et al. 2002). These parameterizations include long and short wave radiation (Chou and Suarez 1994; Chou and Lee 1996) interacting with clouds, which are diagnosed from relative humidity, convective activity (Slingo 1987), Relaxed Arakawa Schubert convection scheme (RAS; Moorthi and Suarez 1992), turbulent mixing and heat and moisture exchanges at the earth's interfaces based on Monin Obukhof similarity theory, non-local vertical diffusion scheme in the planetary boundary layer (Hong and Pan 1996), Oregon State University Land model (Pan and Mahrt 1987), shallow convection (Tiedtke 1983), gravity wave drag (Alpert et al. 1988) and use of smoothed mean orography .

3. Model Climatology

As was noted above, the ability of the coupled model to reproduce climatology and

internal variability is a prerequisite for producing skillful forecasts. An investigation of the deviation between model and observed climatology might be used as one of the strategies for making subsequent improvements. In this section we document the ECPM climatology and deviation from observations, and show that the biases are small and the internal variability is realistic. No artificial flux coupling has therefore been needed.

3.1 Atmospheric Temperature and Winds

Figure 1 shows height-latitude cross-sections of the zonal mean December-January-February (upper left panel) and June-July-August (upper right panel) temperature profiles obtained from the 56 years of ECPM integration and the corresponding model's biases expressed as the difference between the coupled model climatology and the 56 year (1950-2005) R-2 climatology. During the wintertime (lower left panel), the ECPM produces a cold bias in the Northern hemisphere. Warm bias in high latitudes, especially in the Southern hemisphere, accompanies this cold bias. The cold bias in the troposphere has a pronounced maximum at around 700-hPa and might be caused by deficiency in cloud and convection parameterizations. The model's lower stratosphere is colder by around 5º K. These biases are similar to the ones produced by the stand-alone atmospheric model in the AMIP type integration (e.g. Martin et al, 2006), therefore they should be explained by the atmospheric behavior, and not by the coupled processes. The difference in the temperature distribution during boreal summer, JJA is shown in the lower right panel and is qualitatively the same. The warmer near-surface bias shifts towards the equator in the Northern Hemisphere, and the tropical mid-troposphere cold biases are less pronounced.

The temperature biases exhibited in the middle and upper troposphere are somewhat similar to the corresponding biases exhibited by the GFDL Global Coupled Model (GFDL CM2;

Delworth et al. 2006). However, the GFDL CM2 exhibits a pronounced warm bias in the equatorial and tropical parts of the lower troposphere. The ECPM produces colder than observed temperatures in the whole bulk of the tropical troposphere. Overall, the magnitude of the atmospheric temperature errors is larger than the atmospheric model run forced by observed SST (Kanamitsu et al. 2002), reflecting the systematic error in the simulation of SST.

Figure 2 exhibits the systematic error in simulation of climatological SST. In comparison to the NCEP optimum interpolation (OI) SST, the ECPM produced SST 0.5 º – 1º K colder over most of the tropics. On the other hand, the ECPM produces a warmer SST over northern oceans, especially over western and central North Pacific during the summer time. The central Pacific equatorial cold bias is also produced by a number of coupled models including the UCLA global atmospheric model coupled to the GFDL oceanic model (Robertson et al. 1995), GFDL CM2 (Delworth et al. 2006), FSU climate model (Shin et al. 2005) and Hadley Center Climate Model HadGEM1 (Johns et al. 2006).

The systematic errors in the precipitation field are shown in Figure 3. The CPC Merged Analysis of Precipitation (CMAP) for 1979-2004 was used for the observational data. The differences between the ECPM and CMAP are shown in the second from the top row. The corresponding differences between R-2 and CMAP precipitation are shown in the bottom row. The ECPM wintertime Inter Tropical Convergence Zone (ITCZ), shown in the upper panel of the left column of Figure 4, reveals two zonal bands of maximum precipitation (the so-called double ITCZ feature) mainly in the tropical western Pacific. ECPM extends the wintertime double ITCZ feature into the central Pacific as marked by excessive precipitation around 5º N in the central tropical Pacific (on the second from the top left panel of Figure 3). However, as opposed to a number of coupled model climatologies, the double ITCZ feature is not extended all the way into the eastern Pacific. During the summertime (right column on Figure 3), the model

underestimates the western equatorial Pacific precipitation (second from the top right panel), and thus separates the nearly uniform band of maximum precipitation, thus creating the double ITCZ feature in the western Pacific. Comparison with the precipitation from R-2 (third from the top row) indicates that the coupled model produces more realistic wintertime climatology over the northern oceans, than the R-2. This is especially evident over the Kuroshio-Oyashio Extension (KOE) region (second from the top and bottom left panels), where the R-2 DJF precipitation pattern reveals an excessive amount of precipitation. This bias is reduced in the coupled model. It should be noted that the double ITCZ feature is present in almost all of the current coupled models (e.g. Delworth at al, 2006, Johns et al, 2006). As was noted in Johns et al. (2006), this phenomenon may be linked to the equatorial cold bias exhibited by many coupled models. The precipitation biases in the ECPM are comparable to the corresponding biases in GFDL's coupled model (e.g. Figure 17 in Delworth et al, 2006).

The corresponding ECPM zonally averaged zonal winds (not shown here) exhibit biases comparable with the corresponding biases in the GFDL CM2, both for AMIP-type simulation (Anderson et al. 2004) and coupled (Delworth et al. 2006) integrations. The largest discrepancies from the observations (around 10-15 m s^{-1}) occur in the lower stratosphere. These biases are associated with the cold biases in the zonal mean temperature in accordance with the thermal wind equation. In the troposphere, the differences are much smaller,

The error in the Northern Hemisphere zonal wind extends to the surface and is accompanied by a dipole pattern in the sea level pressure bias pattern that consists of an increased surface cyclonic activities in high latitudes, and increased anti-cyclonic activities in mid-latitudes.

The model produces a stationary planetary wave pattern that is similar to the one obtained from R-2 and simulated by GFDL's coupled models. (i.e. Figure 23 Delworth et al, 2006). Similar to GFDL's CM2 global coupled climate models, the ECPM produces weaker troughs

over North Pacific and North-eastern parts of North America, and a weaker ridge over west coast of the United states during boreal winter.

Summarizing, both winter- and summer-time ECPM circulations exhibit systematic biases in comparison to R-2. However, these biases are comparable with the biases produced by other climate models (Anderson et al. 2004; Saha et al. 2006; Delworth et al. 2006).

3.2 Ocean Climatology.

One of the most important variables indicating the potential influence of the ocean on the atmosphere is the integrated heat content from the surface to 400 m depth (see for instance McPhaden 2004) since it can be considered to be a predictor of ENSO development. Therefore, the difference between the model and observed oceanic heat content climatology is an indicator of how good the ocean simulation is. Figure 4 exhibits the annual mean 400 m heat content obtained from the coupled integration (upper row). Difference between the JPL assimilated data and the climatology from the ECPM long-run is shown in the lower panel. The maximum absolute difference between the coupled model run and the assimilated data in the tropics is less than 1.5×10^9 J m^{-2} which is around 10% of the seasonal mean value. The most pronounced differences are seen over the eastern part of the equatorial Pacific and at around 10º North in the Western Pacific. This is a typical bias pattern for coupled model simulations, and is associated with the ITCZ location. ECPM exhibits a positive bias over the KOE region in the western North Pacific. Again, errors of the same size and sign are typical of other coupled models (e.g. Megann 2005). The possible causes of these errors will be discussed later in Section 4.3.

A depth-longitude temperature cross-section along the equator is shown in Figure 5. Again, as for the 400 m heat content, the upper row shows ECPM annual mean simulated data, and the lower row shows the difference between the JPL analysis and the climatology of the

coupled model. The greatest difference can be seen in the western Pacific in the barrier layer below the thermocline. In the eastern Pacific, the model tends to produce deeper thermocline. It should be mentioned, that the absolute values of the discrepancies between the model and assimilated data are small in comparison to the climatology (less than 5% of the absolute values). These biases are qualitatively similar to the ones produced by GFDL's CM2 Global Coupled Climate Models (Wittenberg et al. 2006) and to the biases produced by the Green's function estimate of ocean temperature data (Menemenlis et al. 2005).

To summarize, the ECPM climatology exhibits biases in comparison to observations. However, the amplitudes of these biases are much smaller than the mean values, and the discrepancies are comparable or smaller than the systematic errors produced by most coupled models used for climate prediction (e.g. Sara et al. 2006; Gordon et al. 2000).

4. Internal Variability

In the previous section we documented the mean model state and the deviations from observation. Though correcting these systematic errors could perhaps be made by attempting to tune the model, a more important question is the extent to which the model can reproduce local observed variability as well as remote atmospheric response of various variables. In that regard, the tropical El Nino (ENSO) signal is the most important global signal observed in climate variables. We therefore first checked the ability of the model to produce realistic SST variability in the tropical region.

4.1 Seasonal Cycle in the Tropical Pacific.

Li and Philander, 1996 demonstrated the importance of correct simulations of the annual cycle in the tropical Pacific and it's connection to the mean state. Therefore, the ECPM's ability

to correctly simulate annual variability and phase locking will be studied in this section.

The model's annual cycle (Figure 6, lower left panel) exhibits a semiannual cycle in the western equatorial Pacific, and a westward propagating annual signal in the eastern Pacific. This annual variability is very close to both the HADISST data shown in Jungclaus et. al, (2006) and NCEP OI SSTs shown in Wittenberg et. al, (2006). ECPM outperforms ECHAM5/MPI-OM in reproducing the phase and strength of the equatorial Pacific SSTs. However, similar to GFDL's CM2 global climate models, the ECPM produces stronger than observed annual cycle (see Wittenber et al, 2006, Figure 11a). The corresponding annual mean pattern (upper left panel) is quantitatively in close agreement with observations. There are pronounced warm pool and cold tongue, although the ECPM produces a cold bias over the cold tongue region.

The upper right panel shows the annual mean zonal wind stress. The wind stress pattern is similar to ECMWF reanalysis ERA-40 data (see Wittenberg et al, 2006). The annual mean pattern exhibits easterlies maxima at around 20ºN and 150º-180ºW, and weak westerlies at the equatorial western and eastern boundaries. The lower right panel shows the annual cycle of the zonal wind stress averaged over 2ºS-2ºN. The model captures the westward propagation of the east Pacific signal, as well as the observed relaxation of the trade winds during the spring time. The model reproduces correctly the summertime direction of the wind stress in the eastern Pacific. The model also exhibits realistic seasonality in the interannual variability of ENSO measures by the interannual variance of NINO3.4 index (not shown here). The simulated interannual variance peaks during late autumn and winter, similar to observations.

Another very important phase lock feature is exhibited in the annual cycle of the correlation between NINO3 SST anomalies and Indian Ocean Dipole (IOD). Figure 7 shows the correlation between different indices associated with IOD and NINO3.4 index. The IOD index is based on the difference in SST between the west (10ºS-10ºN, 50º-70ºE) and southeast (5ºS-0º,

90º-110ºE) tropical Indian Ocean. The ENSO signal propagates (via the atmosphere) into the Indian Ocean and results in the substantial correlation between NINO3.4 and western node of the Indian dipole. The amplitudes and phases of the correlations between IOD and NINO3.4 are very similar to observations (e.g. see Figure 19 in Johns et al, 2006). In contrast to the HADGEM1, the ECPM produces a more realistic phase lock between IOD and NINO3.4

4.2 Interannual Variaility.

As was noted in a vast number of studies (e.g. Delworth et al, 2006) the standard deviation of the annual-mean SST can be considered to be one of the the robust measures of the model internal variability. Figure 8 shows the ECPM and NCEP OI SST inter-annual standard deviation. The model SST include 56 years of simulations. The NCEP OI SST was taken for the period of 1950 – 2005. Linear trend was removed from both datasets. The model variability pattern is similar to the observation in the eastern and central tropical Pacific, as well as over the mid-latitude Pacific. As in the case with some other coupled models, e.g. GFDL's CM2 global climate models (Delworth et al, 2006), ECPM exaggerates SST variability, especially in the tropics and over the Oyashio extension region.

To further document the interannual variability in the model, a spectral analysis of the 56 years of the simulated wintertime SST anomalies averaged over NINO3.4 region (5˚N-5˚S, 170˚W-120˚W) (Figure 9) was compared to the spectra of the wintertime NCEP OISST (Reynolds and Smith 1994) from 1950 to 2005. It should be noted that the spectral analysis was performed on a wintertime data due to the pronounced phase lock discussed in the previous section. The ECPM spectra exhibits statistically significant maxima peaks in the 2 to 6-year period interval, which are comparable to analogous peaks obtained from observed NCEP SSTs. These peaks correspond to quasi-periodic ENSO events.

Figure 10 shows wintertime SSTAs averaged over NINO3.4 region. ECPM exhibits

slightly stronger amplitude of variability. This difference is further confirmed by a comparison between the simulated (lower left panel, Figure 10) and observed (lower right panel, Figure 10) frequency distributions of the NINO 3.4 SST anomalies. The probability of the simulated El Nino events is slightly greater than the probability of La Nina events, the amplitude of the warm extreme events in the model is also slightly larger than of the cold events. This is opposite to the simulations by HadGEM1 (Johns et al. 2006) that produces weaker than observed variability for the positive- phase SST anomalies.

4.3 ENSO Evolution

The evolution of ENSO can be expressed by constructing the maps of equatorial SST, wind stress, upper ocean current and temperature lag-regressed onto the NINO3 index (SSTA averaged over 5˚S-5˚N and 150˚-90˚W). Figure 11 shows the ECPM lag regressions onto NINO3 index normalized by one standard deviation. Positive time corresponds to NINO3 leading the variable. All the fields were averaged over 2˚N-2˚S. SSTAs are zonally uniform and nearly steady from 80˚W to 130˚E. The SSTAs peak approximately 12 months after they start to develop in the western Pacific. The SSTAs over the western-most Pacific are negative at the time of the nearly basin-wide peak. These cold anomalies propagate eastward reaching American coast in about 12 months. This behavior is very similar to the observed ER.v2 SST anomalies presented by Wittenberg et al. (2006, Figure 23).

The equatorial zonal wind stress anomalies propagate eastward. However, in comparison to the ECMWF Reanalysis ERA-40 zonal wind stress anomalies (see Wittenberg et al., 2006), there is a steady westerly anomaly pattern over the western part of the equatorial Pacific, up to around 130˚E. This steady pattern is produced by GFDLs coupled models as well and is due to the lack of stochastic noise in the atmospheric forcing (B. Kirtman, personal communications). As in the observations, the peak in the wind stress anomalies over the central Pacific is

preceeded by westerlies over the western Pacific nearly 12 months before the peak. The peak occurs over central Pacific a couple months before the peak in SSTAs. In the ECPM, the easterlies re-appear in the west and central Pacific in 9 months, which is different from the observations that show eastward propagation of easterlies. It should be noted, that the GFDL coupled models do not correctly reproduce this propagation as well.

As in the GFDL/ARCs ocean analysis (Wittenber at al., 2006), ECPM reproduces the eastward propagation of the upper ocean heat content that peaks at the time of the SSTAs peak. However there is a difference in the propagation of the cold upper ocean temperature anomalies from the western Pacific. As is the case with the wind stress anomalies, the cold ocean anomalies re-appear in the central and eastern Pacific, instead of propagating eastward.

The upper ocean eastward zonal currents peak in the eastern-most Pacific 3-12 months before the SSTAs peak. The western currents then start to develop around the ENSO peak. The pattern of westward currents encompasses nearly the whole basin and is centered over the central Pacific. These currents reach maxima 6-9 months after the SSTAs peak. This development is similar to the evolution of GFDL currents (e.g. Wittenberg et al, 2006). Since the zonal current advection of the SST gradient is crucial in transition from El to La Nino, the qualitative similarity between ECPM simulations of the ocean currents and observations is crucial for correct ENSO simulations.

To summarize, the ECPM simulation of ENSO mechanism is qualitatively similar to the observations. The differences are not worse than the ones produced by other (e.g. GFDL) coupled models. We are planning to eventually perform more detailed studies on the cause of these discrepancies.

4.4 ENSO Teleconnection Patterns

As was noted in the variety of studies, the climate system has a global response to the

ENSO forcing. These teleconnection patterns have been extensively studied and documented (e.g. Wallace and Gutzler 1981; Sardeshmukh et al. 2000). The spatial pattern of the SST response is shown in Figure 12. The correlation map between NINO3.4 index and SSTAs over the Pacific produced by the ECPM is qualitatively similar to the observed NCEP OISST map. The meridional strauctures and strength simulated by the model over the Pacific are in good agreement with observations. The weaker signals over Indian and Atlantic oceans are also similar to the observations.

We also studied the skill of ECPM to produce an ENSO related remote atmospheric response by regressing 500-hPa height (Z500) anomalies onto the time series of SST anomalies averaged over NINO3.4 index. The response in Z500 to one standard deviation of the ENSO signal in the ECPM (not shown here) over mid-latitudes bear similarities with the analogous response in R-2 data, indicating that our coupled model reproduces, reasonably well, the atmospheric tropics-midlatitude bridge.

Another test of the skill of a coupled model is its ability to correctly simulate the relationship between SST and heat flux anomalies, especially over North Pacific, and in the tropical monsoon regions, where the atmosphere significantly alters SST variability. We investigated the local correlation between SST anomalies and latent heat fluxes. Figure 13 compares the correlation between SST and latent heat anomalies for ECPM (top panel) and for the AMIP run with the same atmospheric component. This figure can be compared with the Center for Ocean Land Atmosphere (COLA) coupled and stand alone models (Figure 7 from Wu at al. 2006). In comparison to the stand alone SST forced atmospheric integration, the correlation between latent heat flux anomalies and SST anomalies, both the ECPCM and COLA coupled model have negative correlations in the tropical Pacific, and equatorial Indian oceans indicating, that SST anomalies in this regions are forced by the atmosphere. Although the correlations over

the western part of the Pacific warm pool in the coupled model are negative, the region of positive correlations still extends too much to the west in comparison to observations (see map of point-wise correlations derived from GSTTF2 latent heat flux anomalies and observed SST anomalies shown in Figure 6 from Wu at al. 2006). Similar errors occur in the UCLA coupled atmosphere-ocean general circulation model (Yu and Mechoso 1999).However, in comparison to uncoupled run, the introduction of the coupling improves the skill of the heat flux simulation over equatorial Indian Ocean and western tropical Pacific, two regions that are crucial for monsoon development (Wu et al. 2006).

The skill of ECPM in producing the monsoon-ENSO relationship is shown in Figure 14. The figure shows the correlation between June-September precipitation averaged over India (5˚N-25˚N and 60˚-100˚E) and SSTAs during the next winter season (December – February). As was shown in Kirtman and Shukla (2002), the uncoupled AGCMs do not correctly simulate this relationship. Figure 14 shows lots of similarities between simulated by ECPM (upper panel) and observed (lower panel) correlation maps. The observed correlation map was derived from CAMS precipitation data and NCEP OI SSTs. The models correctly captures broad tropical Pacific and Indian Ocean negative correlation pattern. This result is comparable with the correlation pattern produced by COLA ACGCM (Kirtman and Shukla, 2002). Therefore it is safe to say that our coupled model has good skill in simulating Indian monsoon-ENSO relationship.

Due to the lack of disk storage, we did not save daily data for this initial run; thus, we are not able to analyze the skill of simulating higher frequency MJO and storm tracks. However, in the future, we do plan to analyze higher frequency processes in the coupled model.

5. Skill of the Retrospective Forecast

We performed ECPM retrospective forecasts for different months. The initial oceanic

conditions were obtained directly from the JPL ocean analysis. Since we use the same ocean model configuration as the JPL analysis, our model forecast starts smoothly from the ocean analysis, without any noticeable initial shocks. We have now performed one-year predictions starting at the beginning of each month from 1994 to present. The climatology derived from these retrospective forecasts is used to obtain the anomalies for the real-time forecast. The skill of the NINO3.4 predictions, measured by the correlation between the simulated SST NINO3.4 anomalies and the observation (Figure 15), demonstrates that the skill of the forecasts initiated in winter usually drops by the fourth month (spring barrier), but then picks up again and stays high for up to 12 months after the coupled model dynamics starts to influence the predictability. The skill of the forecasts started in summer is very high for up to 9 months lead time. The correlation values smaller than 0.52 (95% confidence level for 12 degrees of freedom) are masked. The ECPM skill seasonal dependency is similar to the one obtained from the NCEP Climate Forecast system (Saha et al 2006). Analogous skill (not shown here) for the North Pacific/North America 500-hPa height also indicates a drop in prediction skill by the 6th month of integration.

Based on this initial ensemble of predictions, we have now started to produce near real-time experimental seasonal forecasts (see http://ecpc.ucsd.edu/COUPLED/CM/coupled.html). Figure 16 demonstrates the relationship between the ECPM SST anomalies forecast and predictions by the dynamical models used for IRI SST anomalies forecasts in the NINO 3.4 region for 2004-2005 forecasts started in May-December. The scatter-plot includes the forecasts from the following models: NASA/NSIPP model, NCEP Coupled Forecast System, Japan Meteorological Agency model , Scripps Institution HCM , Lamont-Doherty model , POAMA (Australian) model , ECMWF model , UKMO model , SNU (Korea) model , ZHANG ICM model , ECHAM/MOM , COLA ANOMALY Model. The data was obtained from http://iri.columbia.edu/climate/ENSO/currentinfo/archive/index.html. The red line indicates a

perfect prediction. The closer the point to the line, the better is the prediction. The IRI models exhibit large scatter in the fourth quadrant, meaning that there is a large error in negative NINO3.4 SST anomalies prediction. The ECPM has smaller errors in the fourth quadrant, as well as smaller scatter around the red line. Again, it should be noted that our forecast skill evaluation is preliminary since it is based on a smaller number of realizations than larger ensemble predictions from the other models.

The skill of 4-6 months lead prediction of DJF (from initial conditions centered at August 1-st) near surface variables (precipitation and 2m temperature), measured by correlation between observed and predicted anomalies, is shown in Figure 17. The correlation coefficients smaller than 95% statistical significance level cutoff are masked. ECPM has some skill in predicting 2m temperature (T2m) over north-western parts of the United States, part of the west coast of Canada and Alaska. The model has a good skill in predicting precipitation over the north-eastern part of the United States and Alaska. For these regions, the model skill is similar to the skill of the FSU climate model coupled to the NCAR Community Land Model Version 2 (CLM2) as discussed in Shin et al. (2005).

Figure 18 shows the skill of the model in 4-6 months lead prediction of the oceanic 400 m heat content and temperature along the equator. The upper panel shows the correlation between December-January-February (DJF) 1994-2005 anomalies predicted from the ECPM integrations started at the beginning of August and the corresponding anomalies from the JPL analysis of the DJF 400 m heat content. Though the correlations are very high over the tropical Pacific Ocean, the ECPM skill is poor over the tropical Indian Ocean.

The corresponding skill in predicting equatorial temperature in the Pacific Ocean is shown in the lower panel of Figure 19. The depth-longitude cross-section of the correlation between ECPM and JPL equatorial DJF temperature anomalies exhibits high skill in predicting oceanic

temperatures over this region.

6. Summary and Further Work

We summarize the description and skill of some prominent coupled models currently being used for seasonal climate predictions in Table 1. The skill is measured by correlation coefficients (for the period of 1994-2005) between predicted wintertime December-January-February (DJF) anomalies (4-6 months lead forecasts initialized in August) and observed DJF anomalies. The Correlation coefficients were averaged over the western United States for 2m temperature and south-eastern United States for precipitation (regions with the correlations greater than 0.5 on the maps on Figure 22). Data for the DEMETER models was obtained from the DEMETER website. Only one ensemble member was used for these calculations. Compared to other models, ECPM exhibits relatively good skill in predicting precipitation and T2m and pcp over the selected United States areas. Again, the main drawback is that we have not yet had the resources to perform many additional ensemble forecasts and due to the availability of JPL assimilation ocean analysis, the forecasts are based only on the 1994-2005 period. However, these preliminary results are promising and provide an indication of the potential of the ECPM. In the future we will compare ECPM with the 11 coupled models that were assessed by Lawrence Livermore National Laboratory's Program for Climate Model Diagnosis and Intercomparison (Philips et al. 2006)

The main reasons why ECPM should now be included into the mix of similar coupled models including the one developed at NCEP are as follows:

- Both ECPC atmospheric and ocean models are very nearly identical to the ones used for data assimilation, thus initial conditions for both atmosphere and ocean are consistent and initial spin-up is small. This is also true for NCEP CFS, NASA NSIPP, COLA and other systems

that perform ocean data assimilation.

- The adjoint of the JPL MIT Ocean model is used routinely to produce a 4-D ocean state assimilation. The consortium for Estimating the Circulation and Climate of the Ocean (ECCO) has already demonstrated the feasibility and utility of providing global, sustained, dynamically sensible estimates for the full three-dimensional, time-varying oceanic state and associated surface forcing fields required to bring the model into consistency with ocean observations. The use of the 4-D variational ocean assimilation system to minimize the initial drift of the ocean model may be an improvement upon the older GFDL assimilation system in use at NCEP.
- The ocean model component is different from that in other coupled models. Different ocean models and assimilation systems are needed to span the natural uncertainty associated with ocean initial conditions and forecasts.
- These global coupled model simulations and forecasts are beginning to be used as boundary conditions for regional coupled model simulations and forecasts. In particular, we are beginning to develop a corresponding regional coupled atmosphere-ocean model that can be used in coastal regions (Seo et al. 2006)

In order to develop the coupled ocean-atmosphere-land model for long lead climate prediction (multi-seasons), we are now planning to further asses the skill of the coupled model retrospective forecasts and compare this skill with the two-tiered prediction model. As was shown, the skill of the forecasts depends on the start date and targeted season, and thus should be similar to the skill found in other coupled models. To get more statistically robust results, especially for individual predictions, we intend to perform 10 member ensemble predictions for each month of the recent 14 years period (t the JPL ocean state analysis is updated monthly and is available from 1993-present). A single initial condition will be used for the ocean initial

condition since only single oceanic initial conditions are available each month. However, the multiple initial conditions for the atmosphere ensemble will be extracted from R-2 from every 12-hour initial state nearest to the beginning of each month.

We will also study the idealized predictability of the coupled model. For this purpose, we intend to perform a long (100 year) 10 member ensemble coupled model simulation without any flux correction. We will use this coupled long simulation as a proxy for an observed state, and perform 2-tier and additional coupled runs with perturbed initial conditions of ocean and atmosphere. We will then compare the statistics from these runs with the original long coupled integration as well as with the actual forecast experiments. This effort could provide a possible upper boundary to coupled predictability, which may then be useful for helping us to better understand the ultimate capability of our coupled model.

Acknowledgments

This study was supported by NOAA NA17RJ1231. The views expressed herein are those of the authors and do not necessarily reflect the views of NOAA. We gratefully acknowledge JPL and NCEP for providing the initial analyses being used for our experimental long-range prediction effort. Special thanks go to Dr D. Stammer and Dr. I. Fukumori and their groups for providing assistance with the MIT ocean model. The computations were performed on PC cluster at SIO, and at NCAR on CSL machines.

References:

Alpert, J.C., M. Kanamitsu, P.M. Caplan, J.G. Sela, G.H. White, and E. Kalnay, 1988: Mountain induced gravity wave drag parameterization in the NMC medium-range model. *Preprints of the Eighth Conference on Numerical Weather Prediction*, Baltimore, MD, American Meteorological Society, 726-733.

Anderson, J., V. Balaji, Anthony J. Broccoli, William F. Cooke, Thomas L. Delworth, Keith W. Dixon, Leo J. Donner, Krista A. Dunne, Stuart M. Freidenreich, Stephen T. Garner, Richard G. Gudgel, C. T. Gordon, Isaac M. Held, Richard S. Hemler, Larry W. Horowitz, Stephen A. Klein, Thomas R. Knutson, Paul J. Kushner, Amy R. Langenhorst, Ngar-Cheung Lau, Zhi Liang, Sergey L. Malyshev, P. C. D. Milly, Mary J. Nath, Jeffrey J. Ploshay, V. Ramaswamy, M. Daniel Schwarzkopf, Elena Shevliakova, Joseph J. Sirutis, Brian J. Soden, William F. Stern, Lori A. Thompson, R. John Wilson, Andrew T. Wittenberg, and Bruce L. Wyman, 2004 : The new GFDL global atmosphere and land model AM2/LM2: Evaluation with prescribed SST simulations, *J Clim*., **17**, 4641-4672

Asselin, R., 1972: Frequency filter for time integrations. *Mon. Wea. Rev*., **100**, 487-490.

Baldwin, M. P. and T. J. Dunkerton, 1999: Downward propagation of the Arctic Oscillation from the stratosphere to the troposphere, *J. Geophys. Res*.**, 104**, 30,937-30,946.

Bishop. J.K.B. and W. B. Rossow, "Spatial and temporal variability of global surface solar irradiance," *J. Geophys. Res.*, **96**,16839-16858

Bourke, W., 1974: a multi-level spectral model. Formulation and hemispheric integrations. *Mon. Wea. Rev*., **102**, 687-701.

Carton, J. A., Gennady Chepurin, Xianhe Cao and Benjamin Giese. 2000: A Simple Ocean Data Assimilation Analysis of the Global Upper Ocean 1950–95. Part I: Methodology. *J. Phys. Oceanog*., **30**, No. 2, pp. 294–309.

Charney J. and J. Shukla, 1981: Predictability of Monsoons. *Monsoon Dynamics*, Edited by James Lighthill and Robert Pearce. Cambridge press.

Chou, M.-D. and M. J. Suarez, 1994: An efficient thermal infrared radiation parameterization for use in General Circulation Models. Technical Report Series on Global Modeling and Data Assimilation, National Aeronautical and Space Administration/TM-1994-104606, 3, 85 pp.

------, and K.-T. Lee, 1996: Parameterizations for the absorption of solar radiation by water vapor and ozone. *J. Atmos. Sci.*, **53**, 1203-1208.

Cox C. M. and B.F. Chao, 2002 Detection of large-scale mass redistribution in the terrestrial sysyetm since 1998, *Science*, **297**, 831-832

Delworth, T. L., A. J. Broccoli, A. Rosati, R. J. Stouffer, V. Balaji, J. T. Beesley, W. F. Cooke, K. W. Dixon, J. Dunne, K. A. Dunne, J. W. Durachta, K. L. Findell, P. Ginoux, A. Gnanadesikan, C. T. Gordon, S. M. Griffies, R. Gudgel, M. J. Harrison, I. M. Held, R. S. Hemler, L. W. Horowitz, S. A. Klein, T. R. Knutson, P. J. Kushner, A. L. Langenhorst, H.-C. Lee, S. J. Lin, J. Lu, S. L. Malyshev, P.C. Milly, V. Ramaswamy, J. Russell, M. D. Schwarzkopf, E. Shevliakova, J. Sirutis, M. Spelman, W. F. Stern, M. Winton, A. T. Wittenberg, B. Wyman, F. Zeng, and R. Zhang, 2006: GFDL's CM2 global coupled climate models--Part 1: Formulation and simulation characteristics. *J. Clim.*, **19**, 643-674

Derber, J. and A. Rosati, 1989: A global oceanic data assimilation system. *J. Phys. Oceanog.*, **19**, 1333-1347.

Dickey, J. O., S. L. Marcus, O. de Viron, and I. Fukumori, 2002. Recent Earth oblateness variations: Unraveling climate and postglacial rebound effects, *Science*, **298**, 1975-1977.

Fukumori, I., 2002: A partitioned Kalman filter and smoother. *Mon. Wea. Rev.*, **130**, 1370-1383.

Gordon, Chris, Claire Cooper, Catherine A Senior, Helene Banks, Jonathan M Gregory, Timothy C Johns, John FB Mitchell, Richard A Wood, 2000: The Simulation of SST, Sea Ice Extents and Ocean Heat Transports in aversion of the Hadley Centre Coupled Model without Flux Adjustments. *Climate Dynamics* **16**, pp 147-168

Ji, M., A. Leetmaa, and J. Derber, 1995: An ocean analysis system for seasonal to interannual climate studies. *Mon. Wea. Rev*., **123**, 460-481.

_____, D. W. Behringer, and A. Leetmaa, 1998: An improved coupled model for ENSO prediction and implications for ocean initialization. Part II: The coupled model. *Mon. Wea. Rev*., **127**, 1022-1034.

Johns TC, Durman CF, Banks HT, Roberts MJ, McLaren AJ, Ridley JK, Senior CA, Williams KD, Jones A, Rickard GJ (2006) The New Hadley Centre Climate Model (HadGEM1): Evaluation of Coupled Simulations. *J. Clim*, **19**: 1327-1353

Juang, H.-M. H. 2004: A Reduced Spectral Transform for the NCEP Seasonal Forecast Global Spectral Atmospheric Model. *Mon. Wea. Rev.* **132**, 1019–1035.

Jungclaus, J.H., N. Keenlyside, M. Botzet, H. Haak1, J.-J. Luo, M. Latif, J. Marotzke, U. Mikolajewicz, and E. Roeckner, 2006: Ocean circulation and tropical variability in the coupled model ECHAM5/MPI-OM, *J. Clim.*, **19**, 3952-3972

Kalnay, E. and M. Kanamitsu, 1988: Time Scheme for Stronglyt Nonlinear Damping Equations. Mon. Wea. Rev., **116**, 1945-1958.

Kalnay, M. Kanamitsu, and W.E. Baker, 1990: Global numerical weather prediction at the National Meteorological Center. *Bull. Amer. Meteor. Soc*., **71**, 1410-1428.

Kanamaru, H. and Masao Kanamitsu, 2006: Scale Selective Bias Correction in a Downscaling of Global Analysis using a Regional Model. *Acceptedd for publication in*

Mon. Wea. Rev.

Kanamitsu, M., 1989: Description of the NMC global data assimilation and forecast system. *Wea. and Forecasting*, **4**, 335-342.

Kanamitsu, M., J.C. Alpert, K.A. Campana, P.M. Caplan, D.G. Deaven, M. Iredell, B. Katz, H.-L. Pan, J. Sela, and G.H. White, 1991: Recent changes implemented into the global forecast system at NMC. *Wea. and Forecasting*, **6**, 425-435.

Kanamitsu, M., A. Kumar, H.-M. H. Juang, W. Wang, F. Yang, J. Schemm, S.-Y. Hong, P. Peng, W. Chen and M. Ji, 2002a: NCEP Dynamical Seasonal Forecast System 2000. *Bull. Amer. Met. Soc*., **83**, 1019-1037.

Kanamitsu, M., W. Ebisuzaki, J. Woolen, J. Potter and M. Fiorino, 2002b: NCEP/DOE AMIP-II Reanalysis (R-2). *Bull. Amer. Met. Soc*. **83**, 1631-1643.

Kanamitsu, M., Cheng-Hsuan Lu, Jae Schemm and W. Ebisuzaki, 2003: The predictability of soil moisture and near surface temperature in hindcasts of NCEP Seasonal Forecast Model. *J. Clim.*, **16**, 510-521.

Kanamitsu, M. and Kingtse, Mo, 2003: Dynamical Effect of Land Surface Processes on Summer precipitation over the Southwestern United States. *J. Clim.*, **16**, 496-509

Kanamitsu, M. and Seong-On Hwang, 2006: Role of Sea Surface Temperature in Reanalysis. *Mon. Wea. Rev*. ***134***, 532-552

Kirtman, B and J. Shukla, 2002: Interactive coupled ensemble: A new coupling strategy for CGCMs. *Geophys. Res.Lett., **29**,1367,*

Large, W. G., J. C. McWilliams, and S. C. Doney, 1994: Oceanic vertical mixing: A review and a model with nonlocal boundary layer parameterization, *Rev. Geophys*., **32**, 363– 403

Leith, C.E., 1971: Atmospheric predictability and two-dimensional turbulence. *J. Atmos. Sci*., **28**, 145-161.

Li, Z., and H.G. Leighton, 1993, Global climatology of the solar radiation budgets at the surface and in the atmosphere from 5 years of ERBE data, *J. Geophy. Res.- Atmosphere*, **98**, 4919-4930.

Li, T. and S.G.H. Philander, 1996: On the annual cycle of the eastern equatorial Pacific. *J. Climate*, **9**, 2986-2998

Marshall, J., A. Adcroft, C. Hill, L. Perelman, and C. Heisey, 1997a: A finite volume, incompressible Navier-Stokes model for studies of the ocean on parallel computers, *J. Geophys. Res*., **102**, 5753– 5766,.

Marshall, J., C. Hill, L. Perelman, and A. Adcroft, 1997b: Hydrostatic, quasihydrostatic and nonhydrostatic ocean modeling, *J. Geophys. Res*., **102**.

Martin, G. M., M.A. Ringer, V.D. Pope, A. Jones, C. Dearden and T.J. Hinton: The physical properties of the atmosphere in the new Hadley Centre Global Environmental Model, HadGEM1. Part 1: Model description and global climatology , *J. Clim.*, **19**, 1274-1301, 2006

McPhaden, M. J., and Coauthors, 1998: The Tropical Ocean-Global Atmosphere observing system: A decade of progress. J. Geophys. Res., **103**, 14 169–14 240.

McPhaden, M.J., 2004: Evolution of the 2002-03 El Niño. *Bull. Am. Meteor. Soc.*, ***85***, 677-695.

Megann, A.P., A.L. New and B. Sinha (2005). Comparisons between the CHIME coupled climate model and HadCM3. *COAPEC Newsletter*, **5**, 7-8.

Menemenlis, D., I. Fukumori, and T. Lee, 2005: Using Green├ s functions to calibrate an ocean general circulation model. *Mon. Wea. Rev*, **133**, 1224-1240.

Moore, A. M. and Kleeman, R. 1996: The dynamics of error growth and predictability in a couple model of ENSO. *Quart. J. Roy. Met. Soc*., **122**, 1405-1446.

Moorthi, S., and M. J. Suarez, 1992: Relaxed Arakawa-Schubert: A parameterization of moist convection for general circulation models. *Mon. Wea. Rev.*, **120**, 978-1002.

Oldenborgh, G. J. van Magdalena A. Balmaseda, Laura Ferranti, Timothy N. Stockdale and David L. T. Anderson. 2005: Did the ECMWF Seasonal Forecast Model Outperform Statistical ENSO Forecast Models over the Last 15 Years?. *J. Clim.*: Vol. **18**, No. 16, pp. 3240–3249.

Geert Jan van Oldenborgh, Magdalena A. Balmaseda, Laura Ferranti, Timothy N. Stockdale and David L. T. Anderson. 2005: Evaluation of Atmospheric Fields from the ECMWF Seasonal Forecasts over a 15-Year Period. *J. Clim*., **18**, 3250–3269.

Hong, S.-Y., H.-L. Pan, 1996: Nonlocal Boundary Layer Vertical Diffusion in a Medium-Range Forecast Model. *Mon. Wea. Rev.*, **124**, 2322-2339.

Pan, H.-L. and L. Mahrt, 1987: Interaction between soil hydrology and boundary layer evelopments. *Boundary Layer Meteor.*, **38**, 185-202.

Phillips, N. A., 1959: Numerical integration of the primitive equation on the hemisphere. *Mon. Wea. Rev.*, **87**, 333-345.

_____, 1974: Application of Arakawa's energy conserving layer model to operational numerical weather prediction. *NMC Office Note 104, August 1975, U. S. Department of Commerce, NOAA, NWS.*

Philips T.J, K, AchutaRao, D Bader, C Covey, C.M. Doutriaux, M.Fiorino,P.J. Gleckler, K.R. Speber and K.E. Taylor, 2006: Coupled Climate Model Appraisal: A benchmark for Future Studies. *EOS, Transactions, American Geophysical Union*, **87,** No. 19, p. 185

Reichler, T. J. and J. O. Roads, 2003: The Role of Boundary and Initial Conditions for Dynamical Seasonal Predictability. *Nonlinear Processes in Geophysics*, **10,** 1-22.

Reichler, T. and John O. Roads. 2004: Time–Space Distribution of Long-Range Atmospheric

Predictability. *J. Atm. Sci.*: Vol. **61**, No. 3, pp. 249–263.

Reichler, T. and J. O. Roads, 2005a: Long-Range Predictability in the Tropics. Part I: Monthly Averages. *J. Clim.*: Vol. **18**, No. 5, pp. 619–633.

Reichler, T. and J. O. Roads, 2005b Long-Range Predictability in the Tropics. Part II: 30–60-Day Variability. *J. Clim*: Vol. **18**, No. 5, pp. 634–650.

Reynolds, R. W., and T. M. Smith, 1994: Improved global sea surface temperature analysis using optimum interpolation. *J. Clim*, **7**, 929-948.

Roads, J.O., S-C. Chen and F. Fujioka, 2001: ECPC's Weekly to Seasonal Global Forecasts. *Bull. Amer. Meteor. Soc*, Vol. **82**, No. 4, 639-658.

Roads, J. 2004: Experimental Weekly to Seasonal U.S. Forecasts with the Regional Spectral Model. *Bulletin of the American Meteorological Society 85(12) Dec 2004.* 1887-1902

Robertson, A.W., C.-C. Ma, C.R. Mechoso and M. Ghil, 1995: Simulation of the tropical Pacific climate with a coupled ocean-atmosphere general circulation model. Part I: The seasonal cycle. *J. Clim.*, **8**, 1178-1198

Robertson, A. W., Upmanu Lall, Stephen E. Zebiak and Lisa Goddard. 2004: Improved Combination of Multiple Atmospheric GCM Ensembles for Seasonal Prediction. *Mon. Wea. Rev.*, Vol. **132**, No. 12, pp. 2732–2744.

Rosati, A., Miyakoda, and R. Gudgel The Impact of Ocean Initial Conditions on ENSO Forecasting with a Coupled Model, *Mon. Wea. Rev.*, Vol. **125**, No. 5, pp. 754–772.

S. Saha, S. Nadiga, C. Thiaw, J. Wang, W. Wang, Q. Zhang, H. M. van den Dool, H.-L. Pan, S. Moorthi, D. Behringer, D. Stokes, G. White, S. Lord, W. Ebisuzaki, P. Peng, P. Xie, 2006: The NCEP Climate Forecast System, *J. Clim.*, **19**, pp. 3483–3517

Sardeshmukh, P.D., G.P. Compo, and C. Penland, 2000: Changes of probability associated with El Nino, *J. Clim*., **13**, 4268-4286

Schopf, P. S., and A. Loughe, 1995: A reduced-gravity isopycnal model: Hindcast of El Nino. *Mon. Wea. Rev.*, **123**, 926-941

Seo, H., A. J. Miller and J. O Roads, 2007: The Scripps Coupled Ocean-Atmosphere Regional (SCOAR) model, with applications in the eastern Pacific sector**,** *J. Clim.*, in press.

Shin, D. W., S. Cocke, T. E. LaRow, and J. J. O'Brien, 2005: Seasonal surface air temperature and precipitation in the FSU climate model coupled to the CLM2, *J. Clim*, **18**, 3217-3228.

Slingo, J.M., 1987: The development and verification of a cloud prediction model for the ECMWF model. *Quart. J. Roy. Meteor. Soc*., **113**, 899-927.

Slingo, A., and J. M. Slingo, 1991: Response of the National Center for Atmospheric Reserch Community Climate Model to Improvements in the Representation of Clouds. *J. Geophys. Res*., **96**, 15,341-15,357.

Stammer, D., C. Wunsch, I. Fukumori and J. Marshall, 2002: State estimation improves prospects for ocean resreach, *EOS, Transactions, American Geophysical Union,* **83**, Nr. 27, p. 289, 294–295

Stammer, D., C. Wunsch, R. Giering, C. Eckert, P. Heimbach, J. Marotzke, A. Adcroft, C.N. Hill and J. Marshall, 2003: Volume, heat and freshwater transports of the global ocean circulation 1993 2000, estimated from a general circulation model constrained by World Ocean Circulation Experiment (WOCE) data . *J. Geophys. Res*., **108**, C1 3007

Straus, D., J. Shukla, Dan Paolino, Siegfried Schubert, Max Suarez, Philip Pegion and Arun Kumar. 2003: Predictability of the Seasonal Mean Atmospheric Circulation during Autumn, Winter, and Spring. *J. Clim*: Vol. **16**, No. 22, pp. 3629–3649.

Tiedtke, M., 1983: The sensitivity of the time-mean large-scale flow to cumulus convection in

the ECMWF model. Proceedings of the ECMWF Workshop on Convection in Large-Scale Models, 28 November-1 December 1983, *European Centre for Medium-Range Weather Forecasts, Reading, England*, 297-316.

Wallace, J.M., and D. Gutzler, 1981: Teleconnection in the geopotential height field during the NorthernHemisphere winter. *Mon. Wea. Rev*., **109**, 784-812.

Wittenberg, A. T., A. Rosati, N-C. Lau, and J. J. Ploshay, 2006: GFDL's CM2 Global Coupled Climate Models. Part III: Tropical Pacific climate and ENSO. *J. Climate*, **19(5)**, 698-722.

Wu, R., B. Kirtman, K. Pegion, 2006: Local Air-sea Relationship in Observations and Model Simulations, *J. Clim.,* **19**, pp. 4914–4932

Xie P., and P. A. Arkin, 1996: Global precipitation: a 17-year monthly analysis based on gauge observations, satellite estimates, and numerical model outputs. *Bull. Amer. Meteor. Soc*., **78**, 2539-2558.

Yu, J.-Y., and C. R. Mechoso, 1999: A discussion on the errors in the surface heat fluxes simulated by a coupled GCM. *J. Clim.,* **12** , 416-426

Zhao, Q., and F. H. Carr, 1997: A prognostic cloud scheme for operational NWP models. *Mon. Wea. Rev*., **125**, 1931-1953.

Figure and Table Captions:

Table 1: Forecast skill of ECPM and DEMETER models in predicting precipitation and 2m temperature over the United States. Skill is measured by correlation coefficients (for the period of 1994-2005) between predicted wintertime December-January-February (DJF) anomalies (4-6 months lead forecasts initialized in August) and observed DJF anomalies. The Correlation coefficients were averaged over the western United States for 2m temperature and south-eastern United States for precipitation (regions with the correlations greater than 0.5 on the maps on Figure 22). Data for the DEMETER models was obtained from the DEMETER website. Only one ensemble member was used for these calculations.

Fig. 1: Height-latitude cross-sections during the Boreal winter (left column) and summer (right column) of the zonal mean temperature profiles obtained from a long integration of the ECPM (upper row). The differences between coupled model simulation and corresponding R-2 data are shown in the lower row. Contour interval of 10º K for the full fields and 1º K for differences. Bold contour in the difference maps shows the zero values.

Fig 2: Boreal winter (left column) and summer (right column) SST obtained from a long integration of the ECPM (upper row). The difference between ECPM simulation and corresponding NCEP OI SST data are shown in lower row. Contour interval is 5º K for the full fields and 0.5º K for differences.

Fig. 3: DJF (left column) and JJA (right column) precipitation obtained from 56-year long ECPM integration (upper row); Difference between ECPM and CMAP climatology (second from the top row) and R-2 precipitation climatology (third from the top row). Difference between R-2 and CMAP climatology (lower row). Contour

interval is 1 mm Day^{-1}

Fig. 4. Annual mean 400m heat content. (upper panel) simulated by ECPM. The lower row shows the difference between JPL MIT assimilated data and ECPM 56-year integration. Contour interval 2 J m-2 for the full fields and 0.5 J m-2 for the differences. Bold contour in the difference maps shows the zero values.

Fig. 5. ECPM Annual mean (upper panel) height-latitude cross-section of the ocean temperature field averaged from 5ºN to 5ºS. The lower row shows the difference between JPL MIT assimilated data and ECPM 56-year integration. Contour interval 2º K for the full field, and 0.2º K for the differences.

Fig. 6: ECPM annual mean SSTs in the tropics (top left panel), contour interval 1˚ K. ECPM annual mean zonal wind stress (multiplied by 10^2) in the tropics (top right), contour interval 2 N m^{-2}. Annual cycle along the equator (2˚N-2˚S) of the deviations from the annual mean ECPM SSTs (lower left), contour interval 0.5˚ K. Lower right: the deviations from the annual mean ECPM zonal wind stress multiplied by 10^2, contour interval 1 N m^{-2}

Fig. 7: Annual cycle of the correlation between IOD index (based on the difference in SST between the west (10˚S-10˚N, 50˚-70˚E) and southeast (5˚S-0˚, 90˚-110˚E) tropical Indian Ocean), west and south east nodes of the dipole index and NINO3.4.

Fig 8: Standard deviation of the annual-mean SST (K). Left: ECPM 56 years of simulations. Right: NCEP OI SST for the period of 1950-2005. Contour interval 0.1˚ K

Fig. 9: Spectral analysis of the wintertime NINO3.4 (5˚N-5˚S, 170˚W-120˚W) ECPM SSTAs obtained from the 56-year integration (solid red line) and NCEP/DOE OI SSTAs for 1950-2005 period (solid green line). The corresponding red noise spectra (dashed

magenta line for ECPM and dashed blue for OISST) indicate the significance of the power peaks.

Fig. 10: Upper panel: wintertime SSTAs averaged over NINO3.4 region simulated by ECPM (solid line) and NCEP OISST (dashed line). Lower row: frequency distribution of the NINO3.4 SSTAs in ECPM (left panel) and NCEP OI SST data (right panel). 56 years of ECPM simulations were used. NCEP OISST data is for 1950-2005 time period

Fig. 11: ECPM lag -regression maps obtained by regressing onto the normalized NINO3 index. From left to right: SST (units [K K^{-1}]), zonal wind stress anomalies(N m^{-2} K^{-1}), upper ocean temperature averaged over upper 250 m([K K^{-1}]), upper ocean zonal current averaged over upper 50m ([m s^{-1} K^{-1}]). All fields are averaged over 2ºS-2ºN. The time goes from -18 months to +18 month. Positive time means that NINO3 index is leading.

Fig. 12: Correlation between NINO3.4 and SSTAs. Left: ECPM; right: NCEP OI SSTAs. Contour interval 0.1.

Fig. 13: Correlation between SST and latent heat anomalies from ECPM (top panel) and from AMIP GSM integration data (bottom panel). Interval is 0.1

Fig. 14: Correlation between Indian summer (June-September) monsoon rainfall and the subsequent winter season DJF SSTAs. Top: ECPM; Bottom: CAMS precipitation and NCEP OI SSTs.

Fig. 15: The skill of the NINO3.4 predictions measured by the correlation between ECPM and NCEP/DOE OI NINO3.4 SST anomalies Correlations coefficients that are less than 95% significance level cutoff are masked

Fig. 16: Scatter plot of NINO3.4 SST anomalies predictions (2004-2005) started in May-December versus NCEP/DOE OI SSTAs. The red line indicates perfect prediction, the closer the point to the line, the better the prediction. The IRI models exhibit large

scatter in the fourth quadrant, meaning that there is a large error for negative NINO3.4 SST anomaly predictions. ECPM has smaller errors in the fourth quadrant, as well as smaller scatter about the red line.

Fig. 17: Skill of the 4-6 months lead DJF prediction of near surface variables: precipitation and 2m temperature (T2m) from forecasts started at the beginning of August for the 1994-2005 time period. Correlations coefficients that are less than 95% significance level cutoff are masked.

Fig. 18: Upper panel: the correlation between DJF 1994-2005 anomalies predicted from the ECPM integrations started in August and the corresponding anomalies from the JPL analysis of the DJF 400 m heat content. Contour interval 0.1 Lower panel: same as upper panel but for the depth-longitude cross-section of the correlation between ECPM and JPL equatorial DJF temperature anomalies. Contour interval 0.1. Correlations coefficients that are less than 95% significance level cutoff are masked

Table 1. Skill (measured by correlation) of coupled model predictions for the US regions

Model	***Ocean***	***Atmosphere***	***4-6 months lead skil:l precip***	***4-6 months lead skill: T2m***
CERFACS	OPA8.2 2x2, L31	ARPEGE T63, L31	0.5	0.7
ECMWF	HOPE-E; 1.4x0.3-1.4, L29	IFS, T95, L40	0.5	0.7
LODYC	OPA8.2 2x2, L31	IFS, T95, L40	0.7	0.5
Met Office	OGCM based on HadCM3; 1.25x0.3-1.25, L40	HadAM3, 2.5x3.75, L19	0.7	0.5
MPI	MPI, 1.5x1.5 L40	ECHAM5, T63L31	0.6	0.4
ECPM	MIT 1x1/3-1, L46	GSM T62, L28	0.6	0.7

Forecast skill of ECPM and DEMETER models in predicting precipitation and 2m temperature over the United States. Skill is measured by correlation coefficients (for the period of 1994-2005) between predicted wintertime December-January-February (DJF) anomalies (4-6 months lead forecasts initialized in August) and observed DJF anomalies. The Correlation coefficients were averaged over the western United States for 2m temperature and south-eastern United States for precipitation (regions with the correlations greater than 0.5 on the maps on Figure 22). Data for the DEMETER models was obtained from the DEMETER website. Only one ensemble member was used for these calculations.

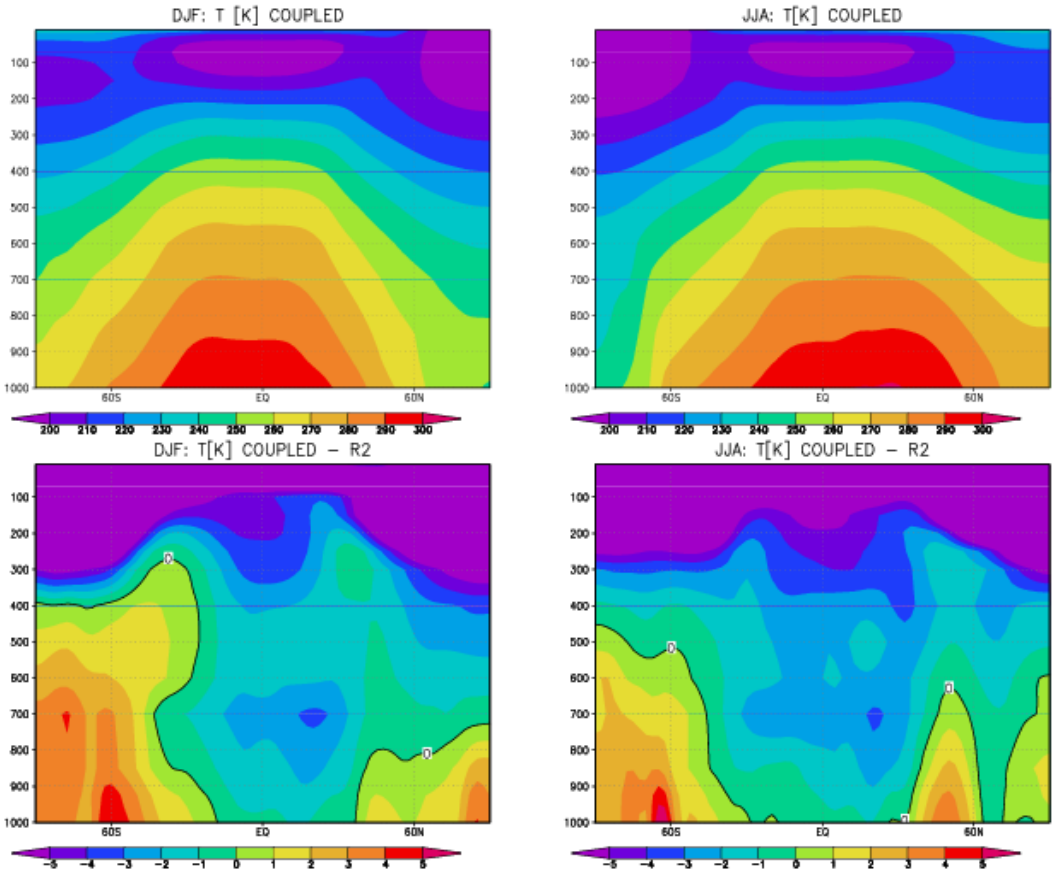

Fig. 1: Height-latitude cross-sections during the Boreal winter (left column) and summer (right column) of the zonal mean temperature profiles obtained from a long integration of the ECPM (upper row). The differences between coupled model simulation and corresponding R-2 data are shown in the lower row. Contour interval of 10º K for the full fields and 1º K for differences. Bold contour in the difference maps shows the zero values.

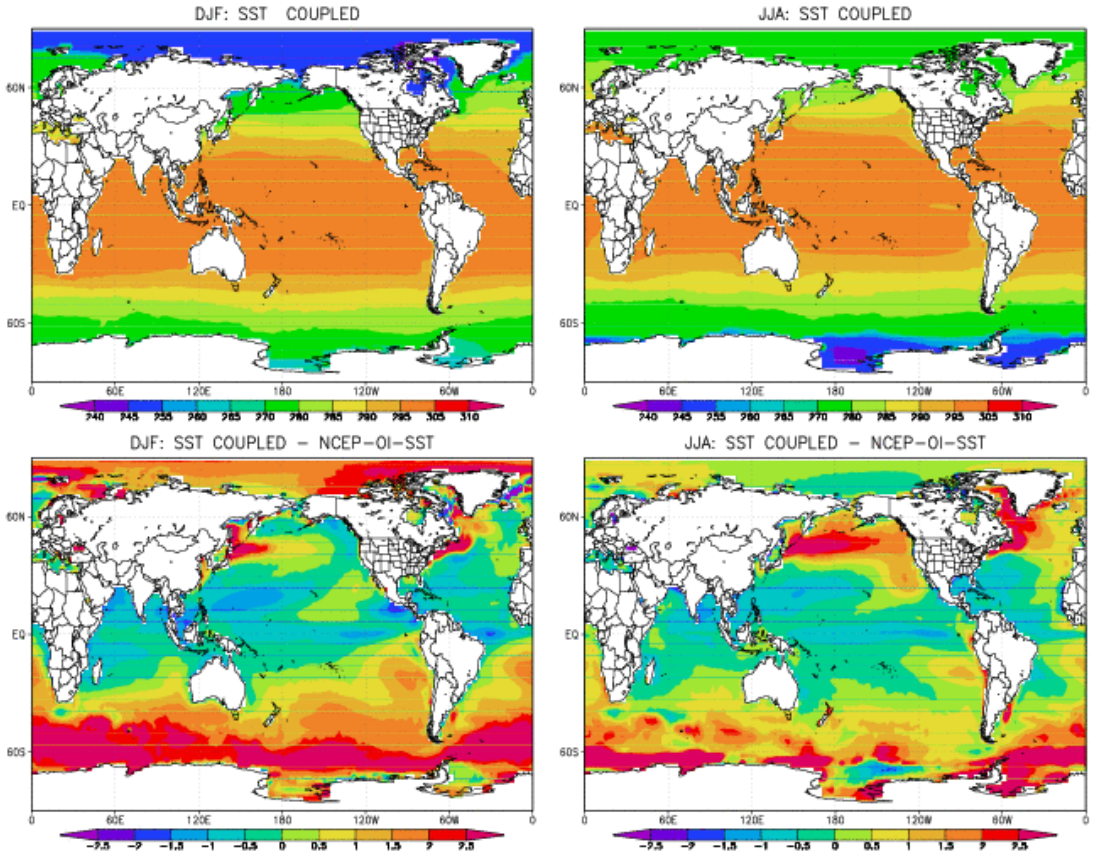

Fig 2: Boreal winter (left column) and summer (right column) SST obtained from a long integration of the ECPM (upper row). The difference between ECPM simulation and corresponding NCEP OI SST data are shown in lower row. Contour interval is 5º K for the full fields and 0.5º K for differences.

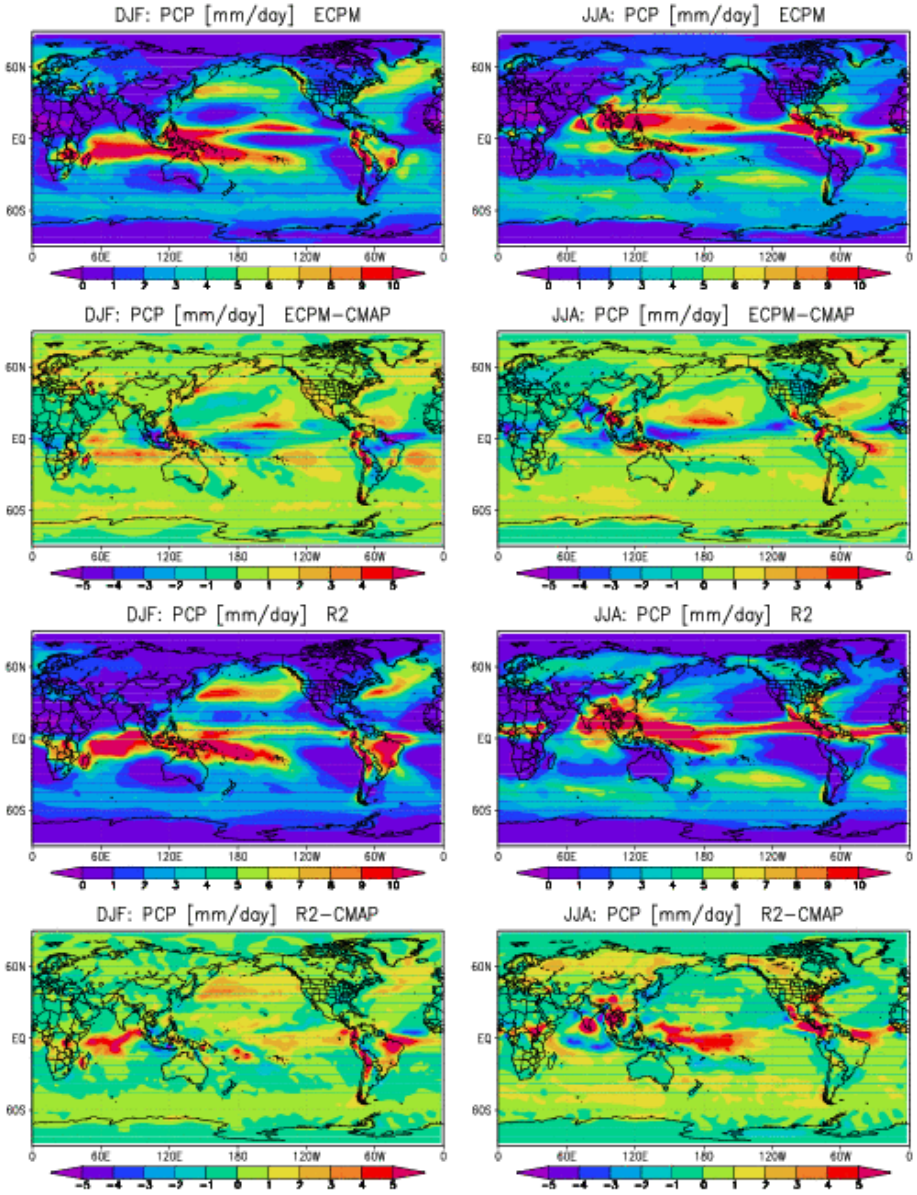

Fig. 3: DJF (left column) and JJA (right column) precipitation obtained from 56-year long ECPM integration (upper row); Difference between ECPM and CMAP climatology (second from the top row) and R-2 precipitation climatology (third from the top row).
Difference between R-2 and CMAP climatology (lower row). Contour interval is 1 mm Day^{-1}

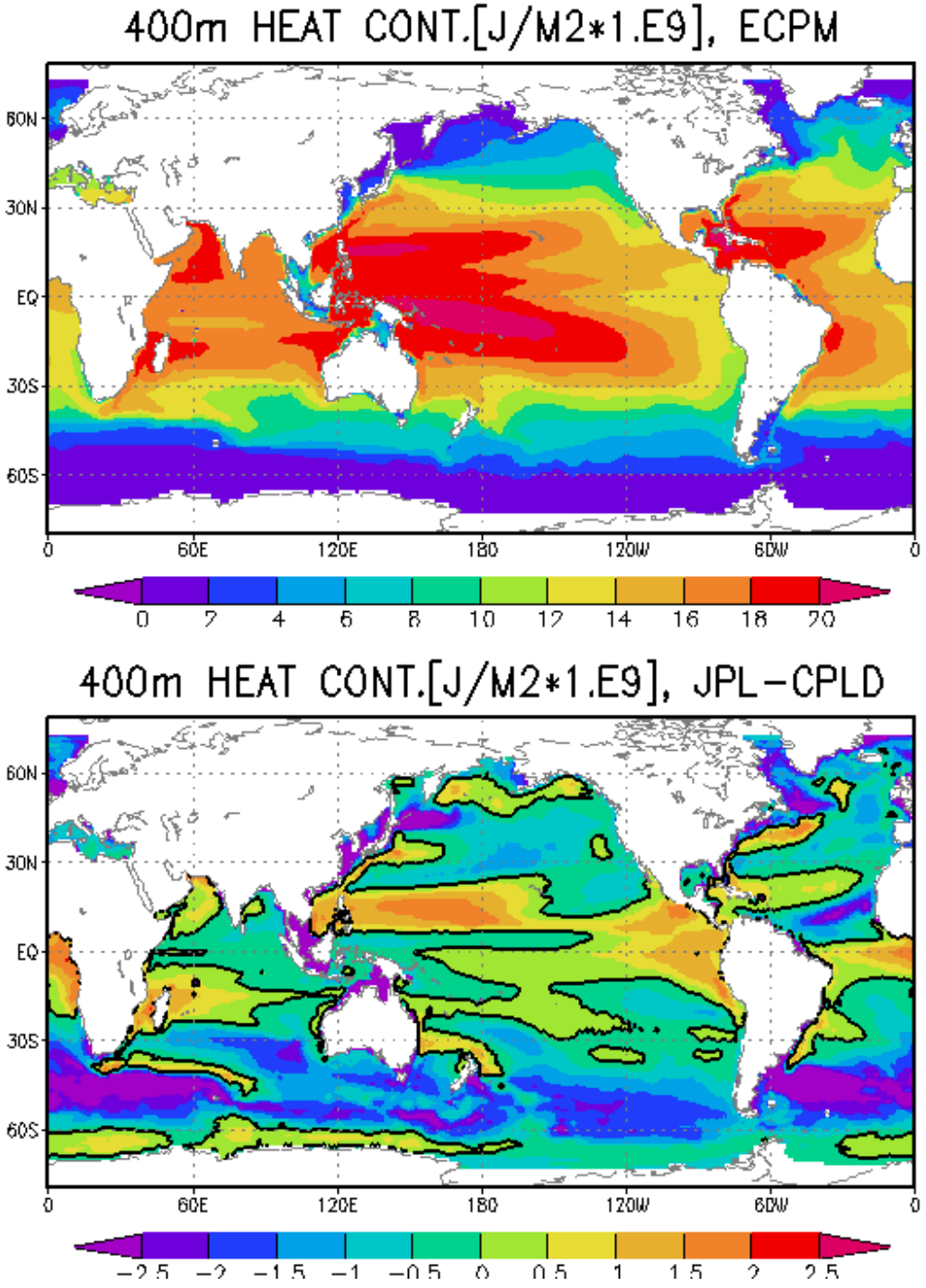

Fig 4: Annual mean 400m heat content. (upper panel) simulated by ECPM. The lower row shows the difference between JPL MIT assimilated data and ECPM 56-year integration. Contour interval 2 J m^{-2} for the full fields and 0.5 J m^{-2} for the differences. Bold contour in the difference maps shows the zero values.

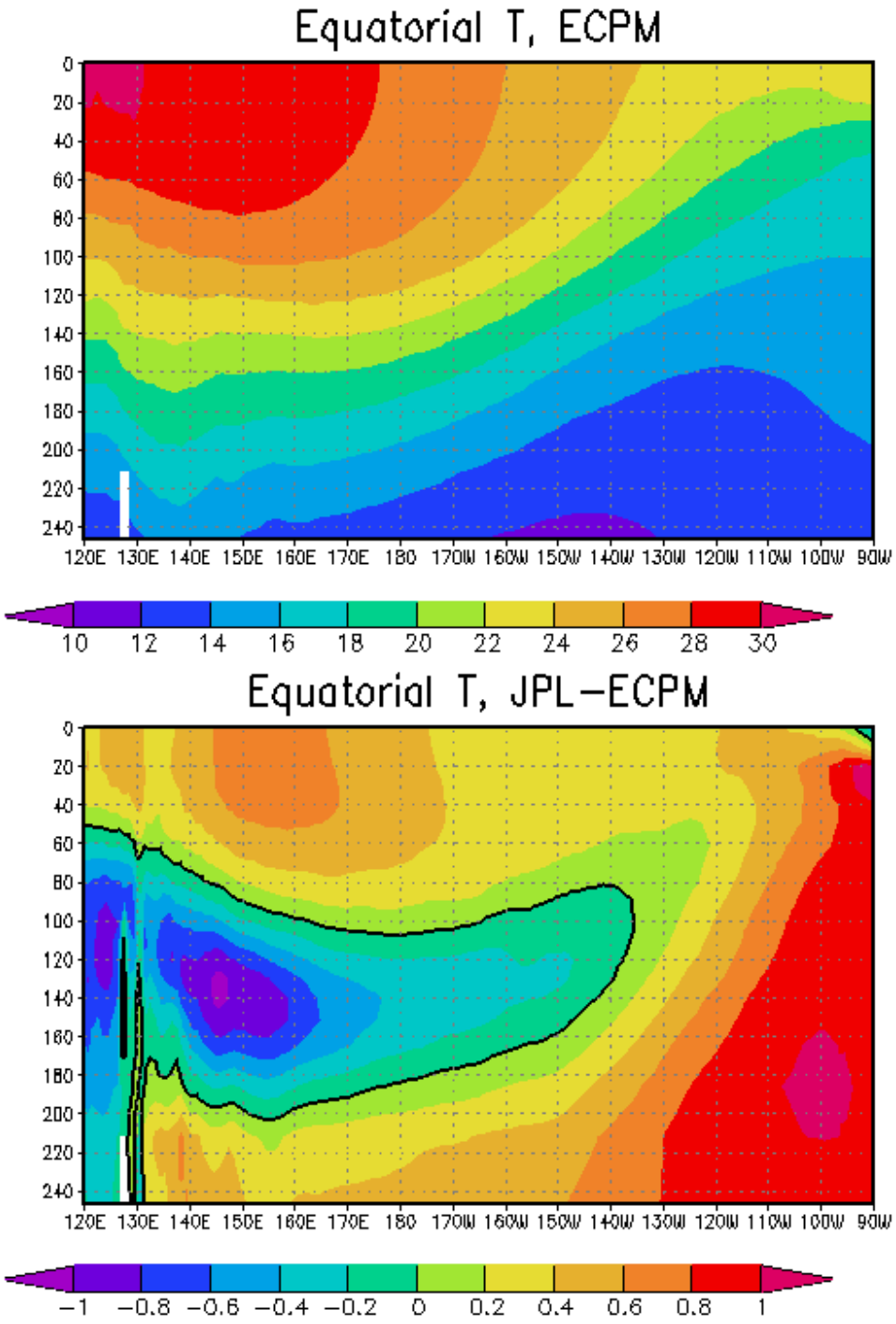

Fig.5: ECPM Annual mean (upper panel) height-latitude cross-section of the ocean temperature field averaged from 5ºN to 5ºS. The lower row shows the difference between JPL MIT assimilated data and ECPM 56-year integration. Contour interval 2º K for the full field, and 0.2º K for the differences.

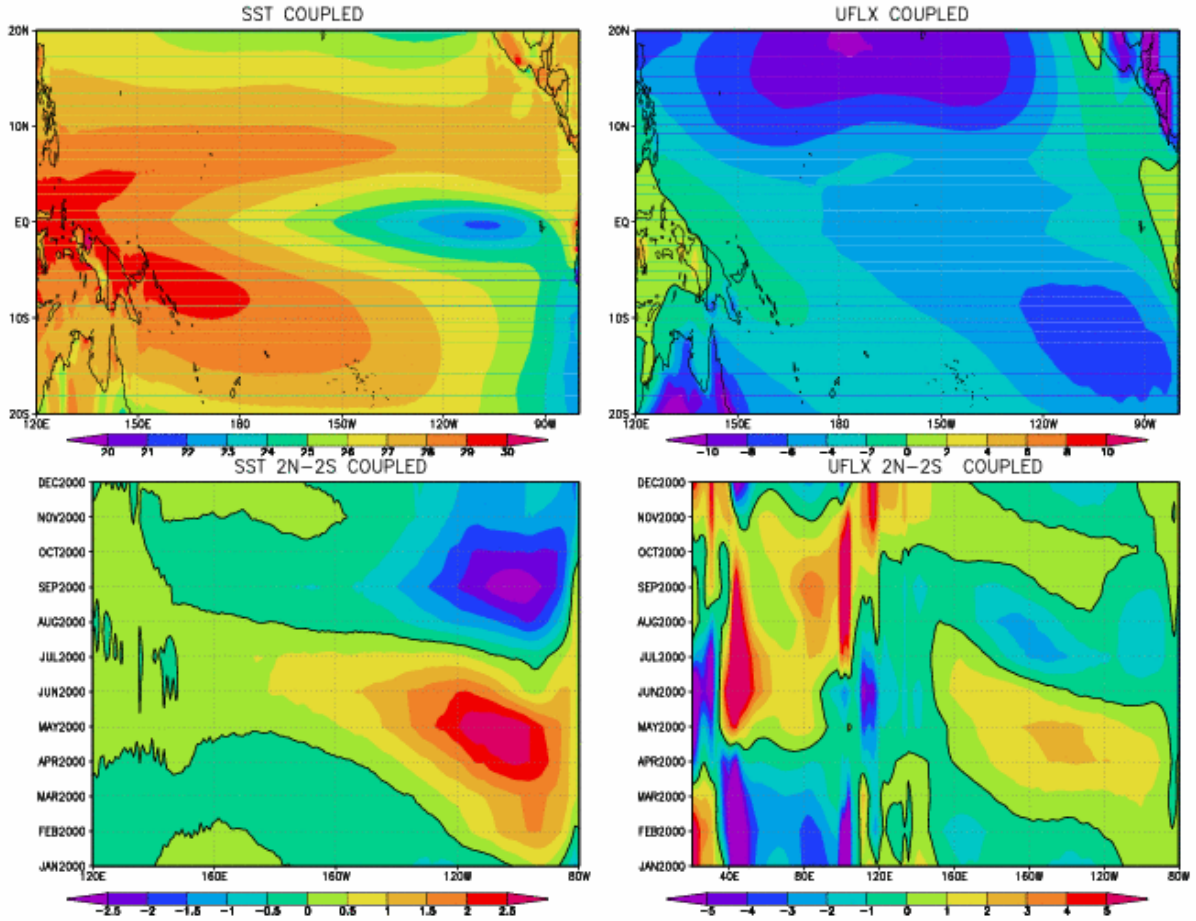

Fig. 6: ECPM annual mean SSTs in the tropics (top left panel), contour interval 1˚ K. ECPM annual mean zonal wind stress (multiplied by 10^2) in the tropics (top right), contour interval 2 N m^{-2}. Annual cycle along the equator (2˚N-2˚S) of the deviations from the annual mean ECPM SSTs (lower left), contour interval 0.5˚ K. Lower right: the deviations from the annual mean ECPM zonal wind stress multiplied by 10^2, contour interval 1 N m^{-2}.

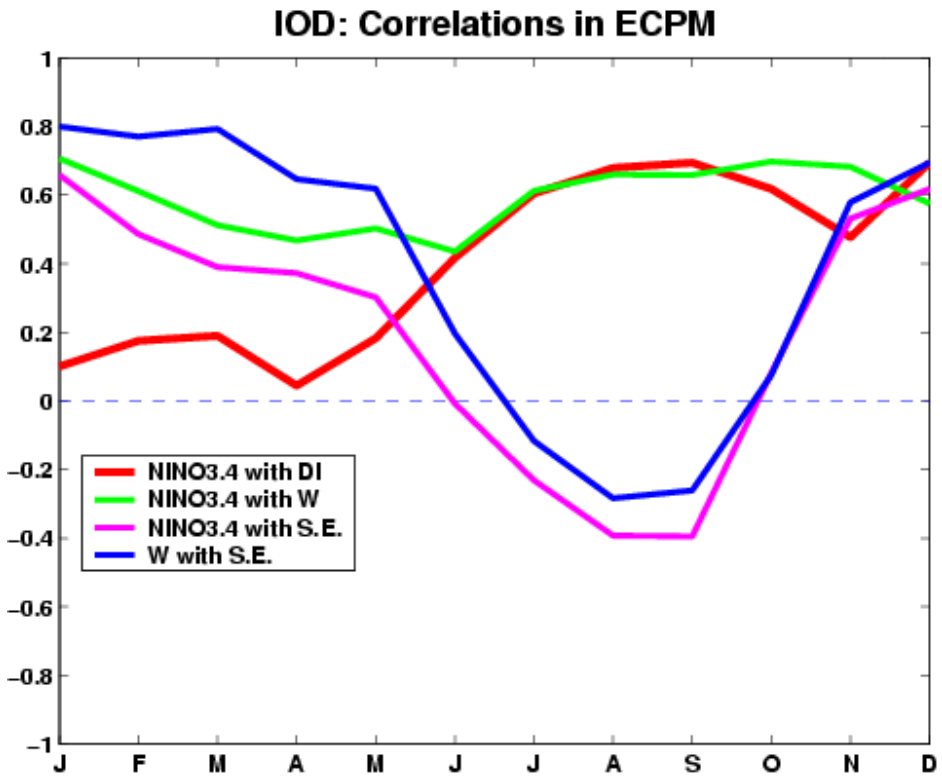

Fig. 7: Annual cycle of the correlation between IOD index (based on the difference in SST between the west (10˚S-10˚N, 50˚-70˚E) and southeast (5˚S-0˚, 90˚-110˚E) tropical Indian Ocean), west and south east nodes of the dipole index and NINO3.4.

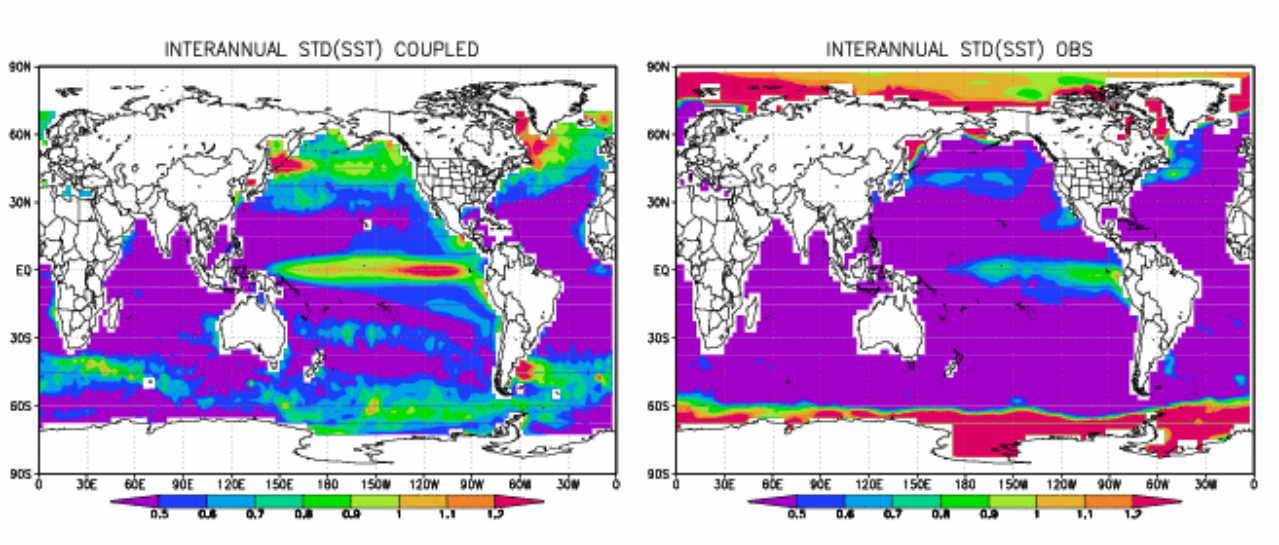

Fig 8: Standard deviation of the annual-mean SST (K). Left: ECPM 56 years of simulations. Right: NCEP OI SST for the period of 1950-2005. Contour interval 0.1 K

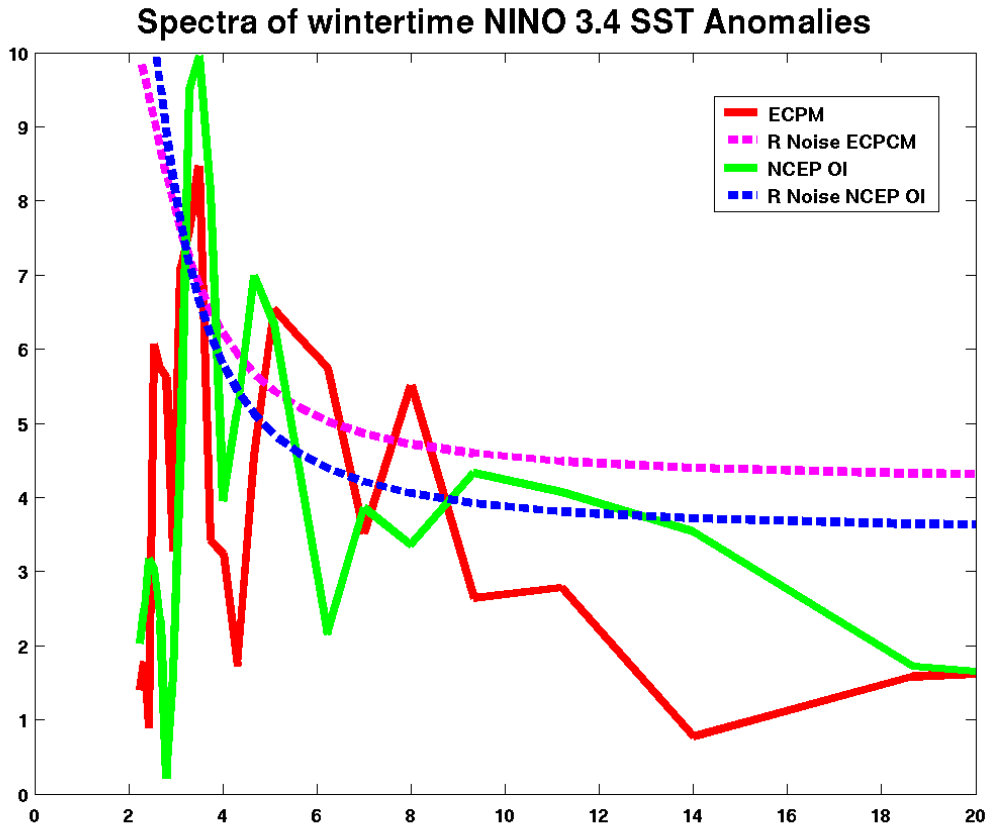

Fig. 9: Spectral analysis of the wintertime NINO3.4 (5˚N-5˚S, 170˚W-120˚W) ECPM SSTAs obtained from the 56-year integration (solid red line) and NCEP/DOE OI SSTAs for 1950-2005 period (solid green line). The corresponding red noise spectra (dashed magenta line for ECPM and dashed blue OISST) indicate the significance of the power peaks.

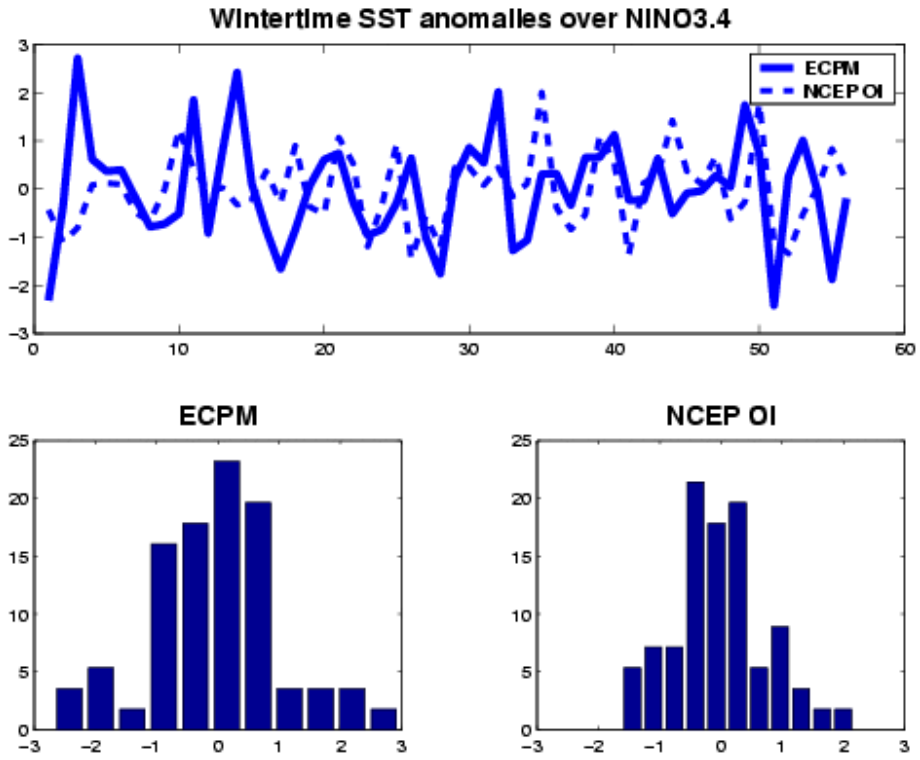

Fig. 10: Upper panel: wintertime SSTAs averaged over NINO3.4 region simulated by ECPM (solid line) and NCEP OISST (dashed line). Lower row: frequency distribution of the NINO3.4 SSTAs in ECPM (left panel) and NCEP OI SST data (right panel). 56 years of ECPM simulations were used. NCEP OISST data is for 1950-2005 time period

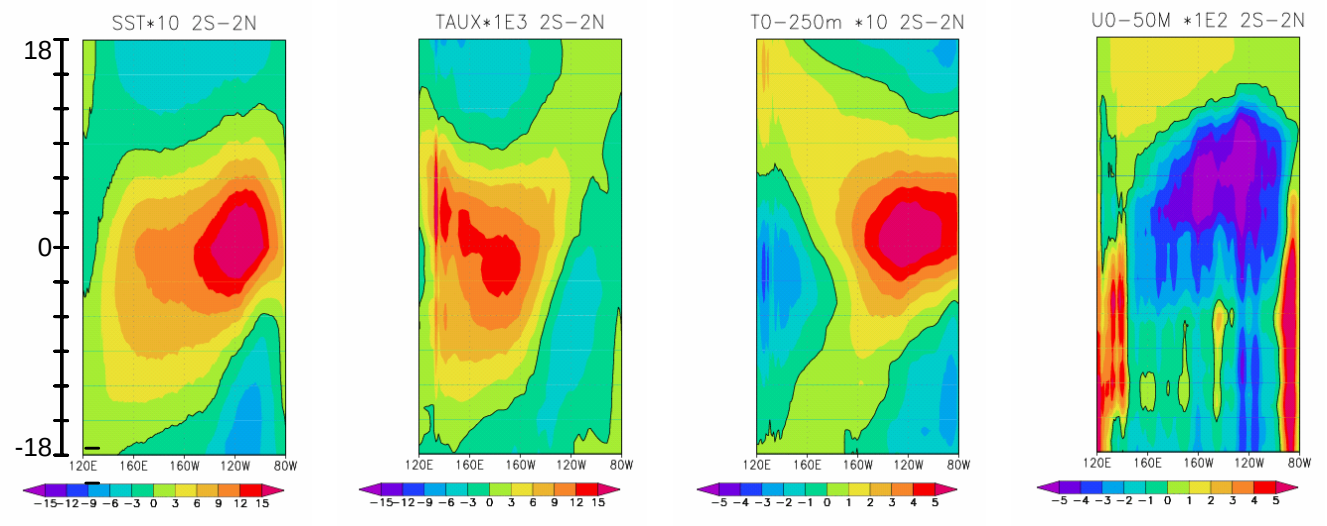

Fig. 11: ECPM lag -regression maps obtained by regressing onto the normalized NINO3 index. From left to right: SST (units [K K^{-1}]), zonal wind stress anomalies(N m^{-2} K^{-1}), upper ocean temperature averaged over upper 250 m([K K^{-1}]), upper ocean zonal current averaged over upper 50m ([m s^{-1} K^{-1}]). All fields are averaged over 2ºS-2ºN. The time goes from -18 months to +18 month. Positive time means that NINO3 index is leading.

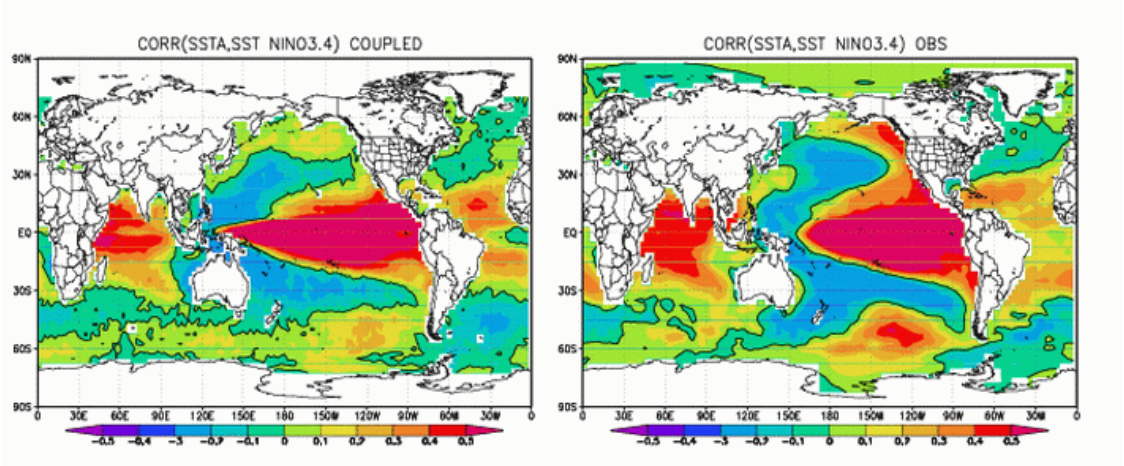

Fig. 12: Correlation between NINO3.4 and SSTAs. Left: ECPM; right: NCEP OISSTAs. Contour interval 0.1

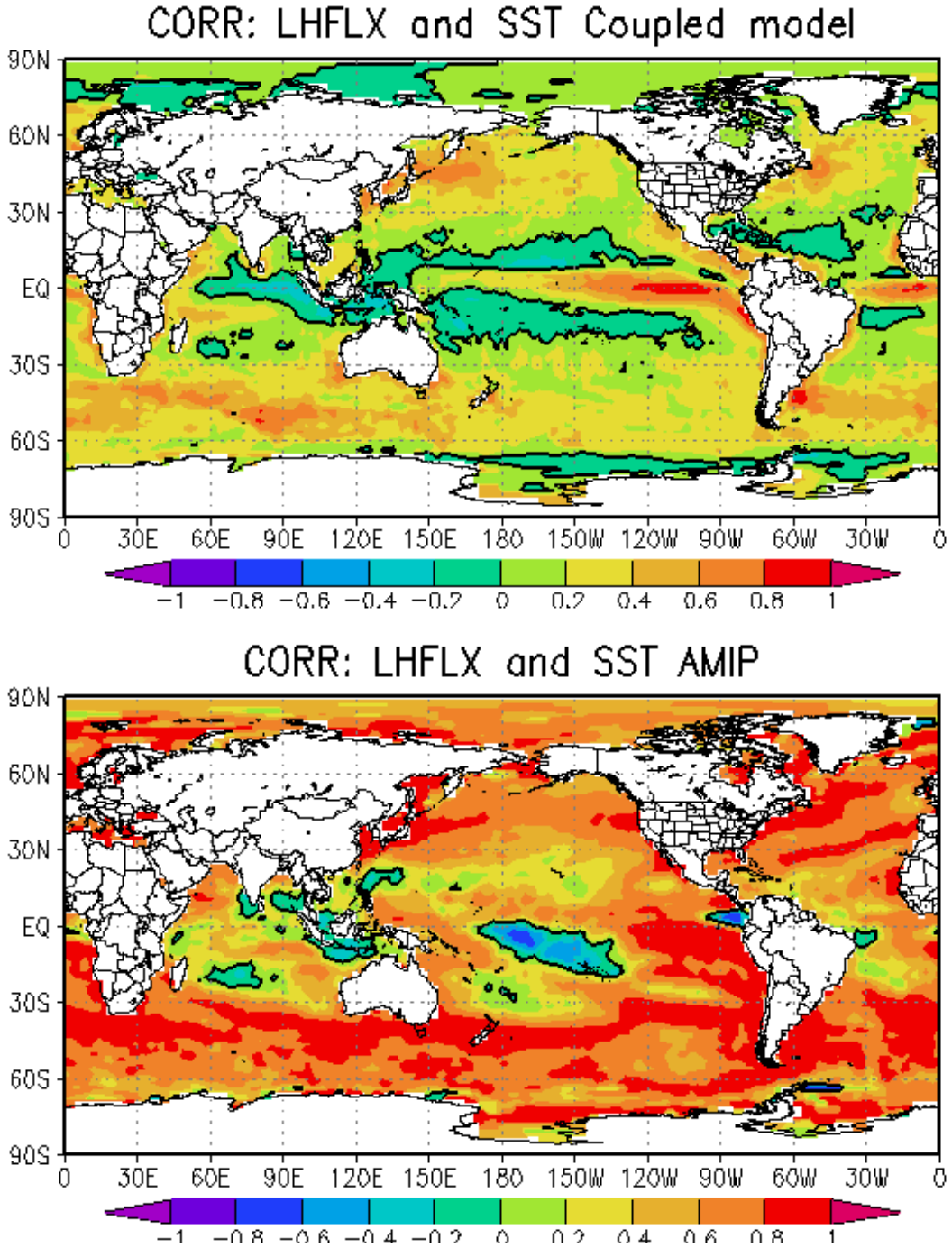

Fig 13: Correlation between SST and latent heat anomalies from ECPM (top panel) and from AMIP GSM integration data (bottom panel). Interval is 0.2

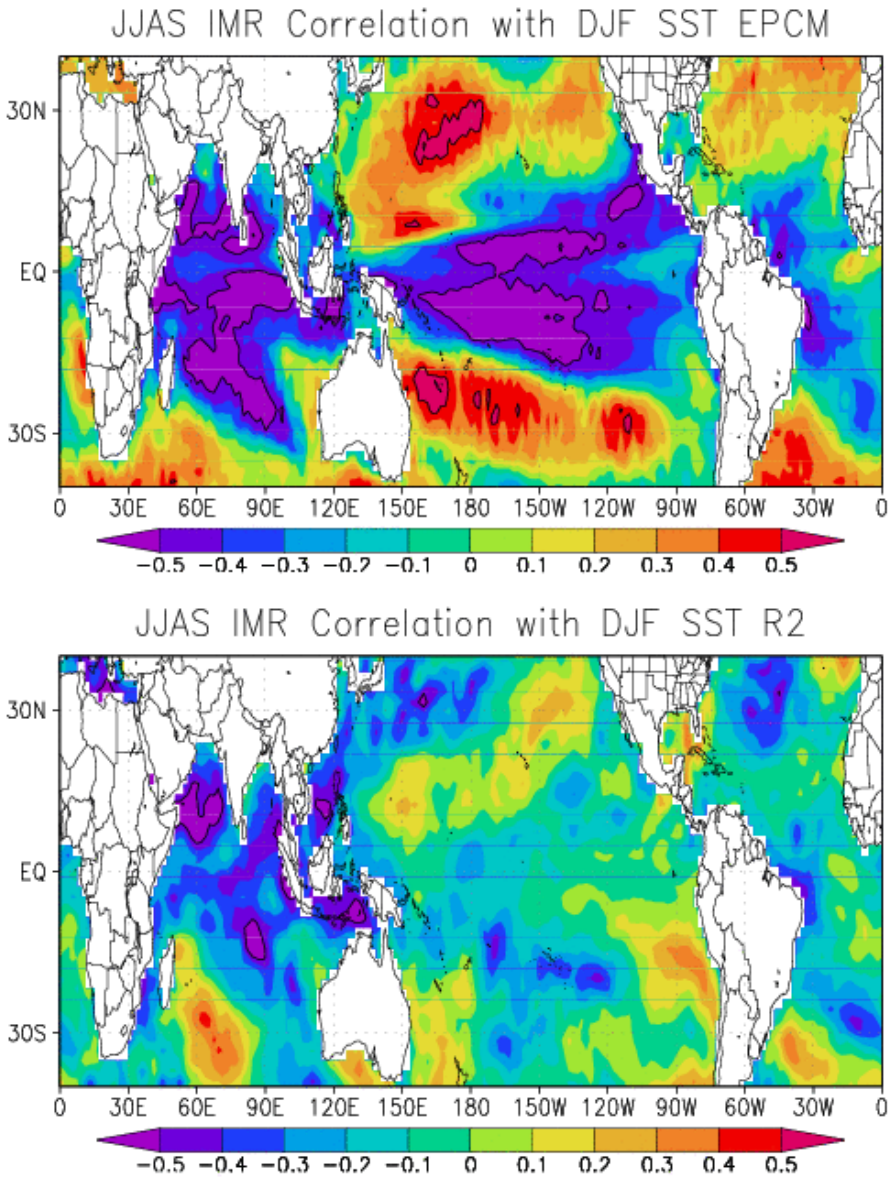

Fig. 14: Correlation between Indian summer (June-September) monsoon rainfall and the subsequent winter season DJF SSTAs. Top: ECPM; Bottom: CAMS precipitation and NCEP OI SSTs.

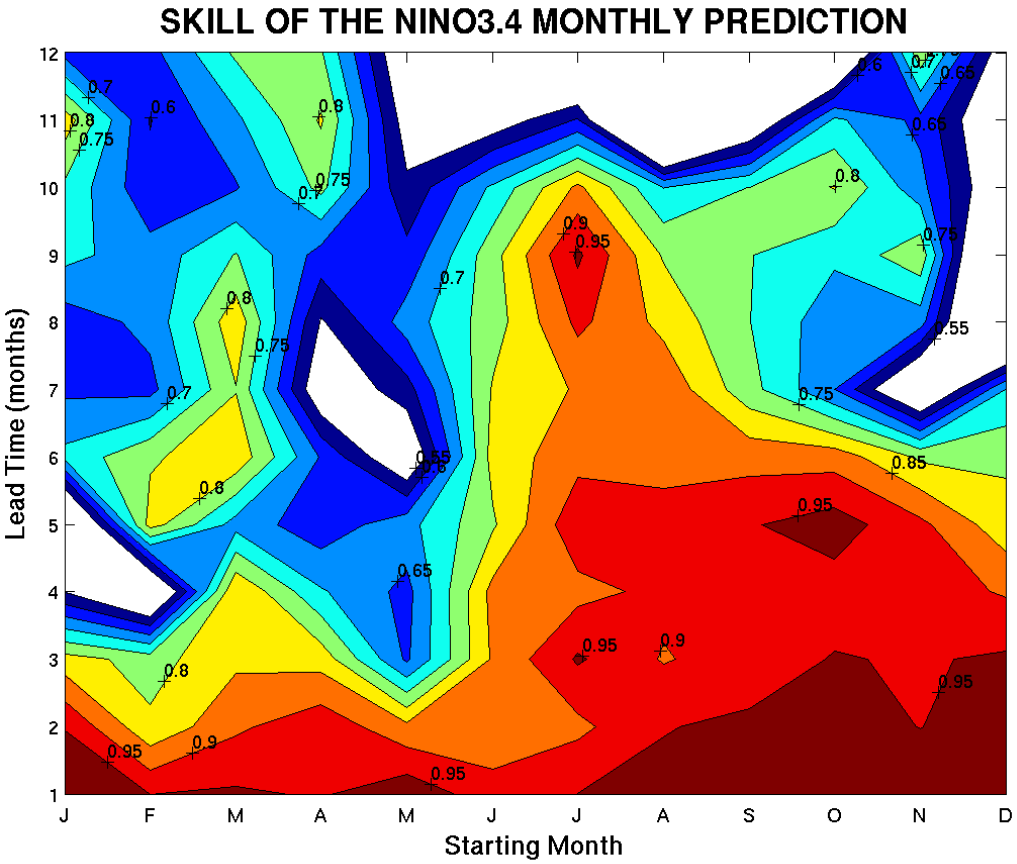

Fig. 15: The skill of the NINO3.4 predictions measured by the correlation between ECPM (1994-2005) and NCEP/DOE OI NINO3.4 SST anomalies Correlations coefficients that are less than 95% significance level cutoff are masked

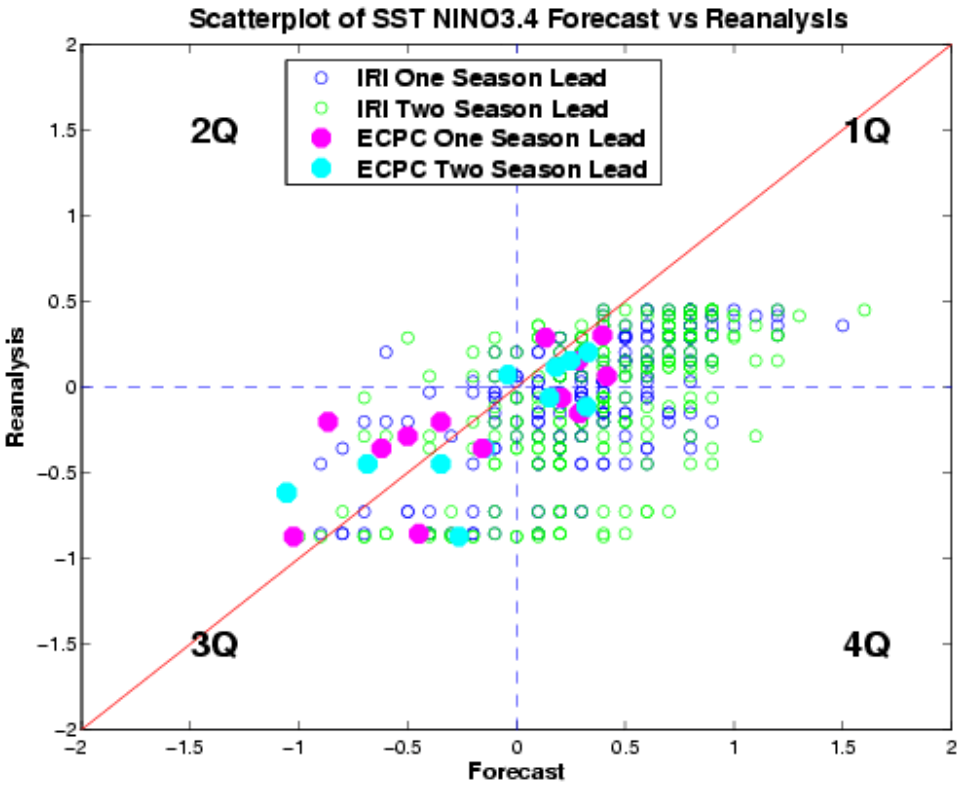

Fig. 16: Scatter plot of NINO3.4 SST anomalies predictions (2004-2005) started in May-December versus NCEP/DOE OI SSTAs. The red line indicates perfect prediction, the closer the point to the line, the better the prediction. The IRI models exhibit large scatter in the fourth quadrant, meaning that there is a large error for negative NINO3.4 SST anomaly predictions. ECPM has smaller errors in the fourth quadrant, as well as smaller scatter about the red line.

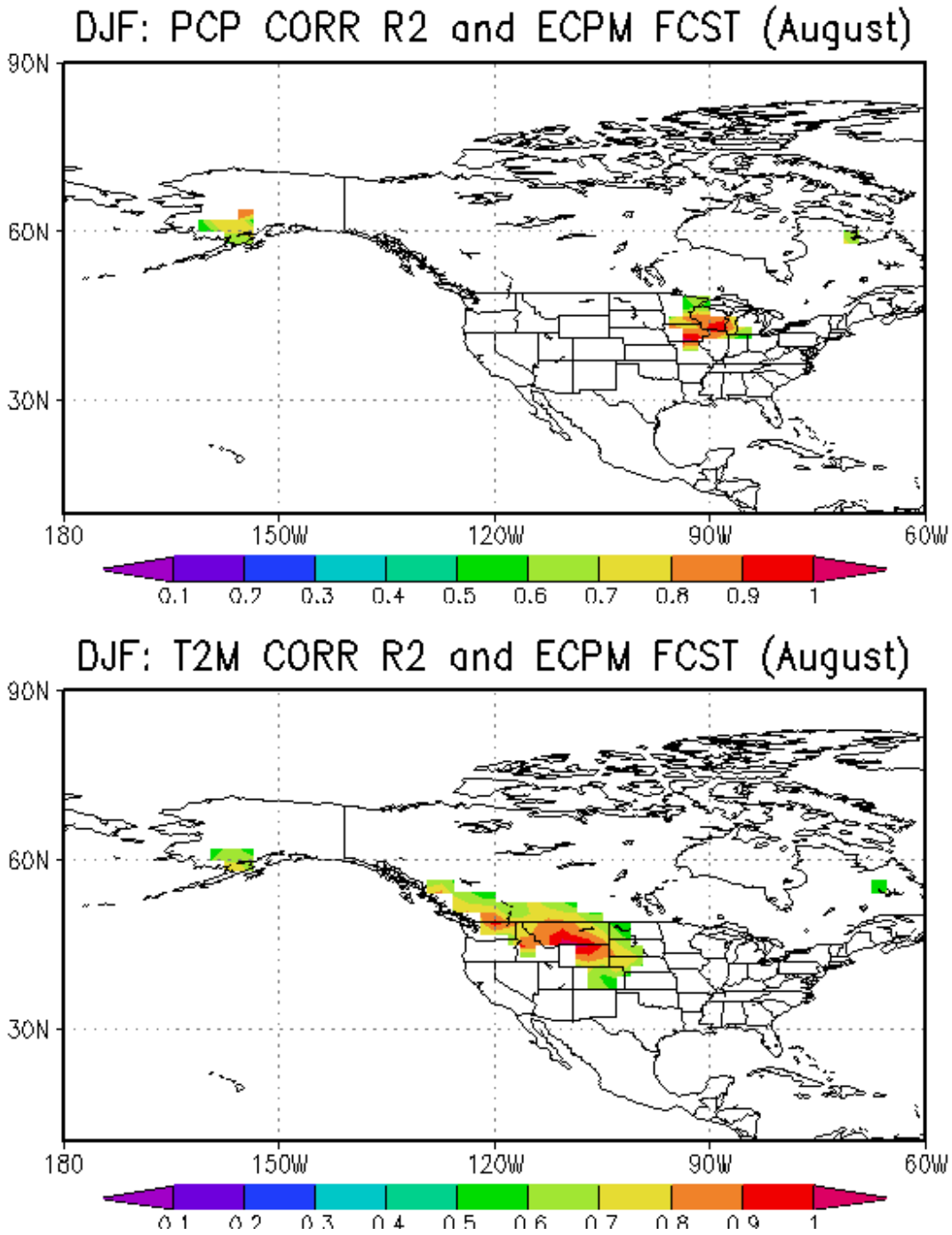

Fig. 17: Skill of the 4-6 months lead DJF prediction of near surface variables: precipitation and 2m temperature (T2m) from forecasts started at the beginning of August for the 1994-2005 time period. Correlations coefficients that are less than 95% significance level cutoff are masked

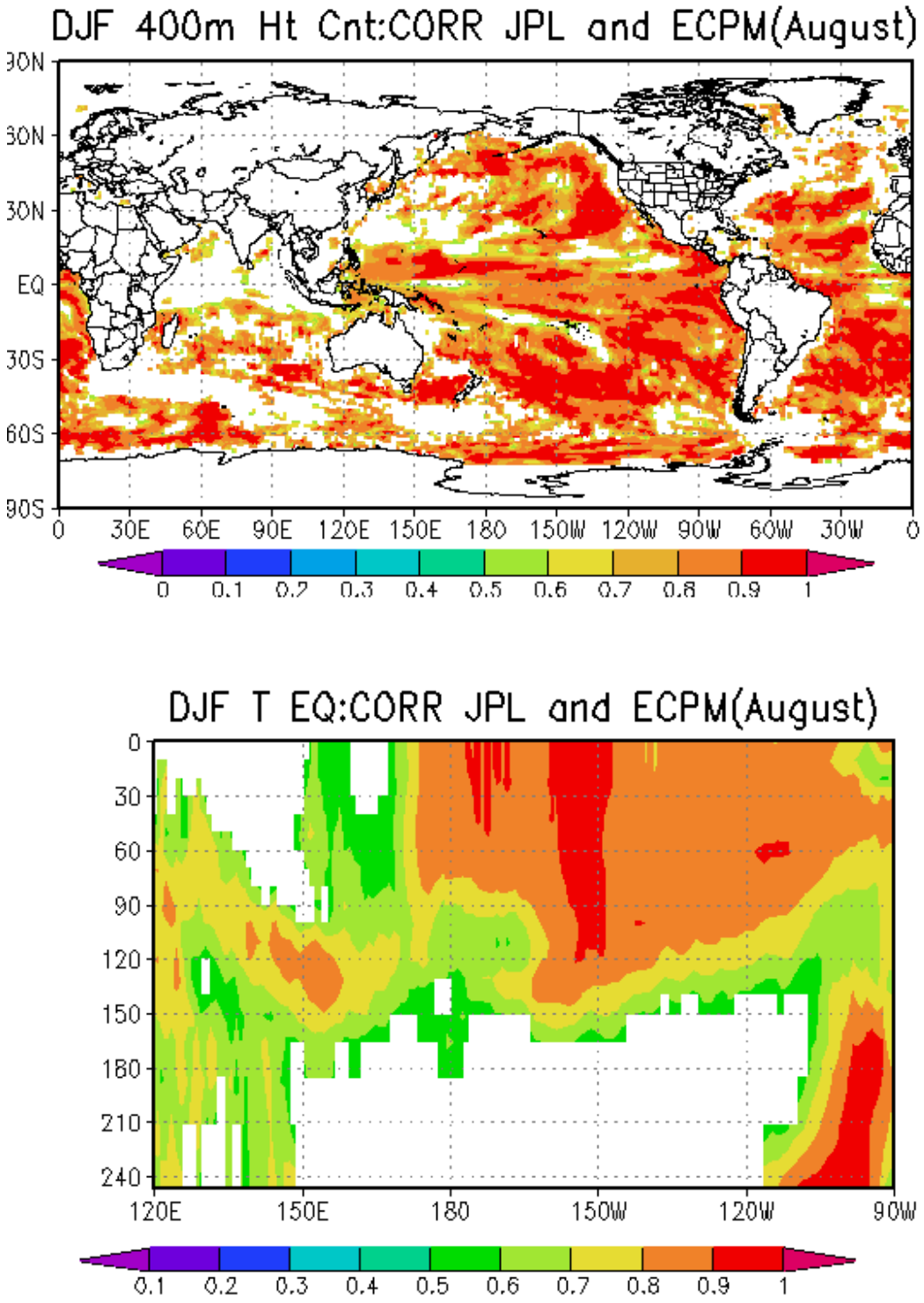

Fig. 18: Upper panel: the correlation between DJF 1994-2005 anomalies predicted from the ECPM integrations started in August and the corresponding anomalies from the JPL analysis of the DJF 400 m heat content. Contour interval 0.1 Lower panel: same as upper panel but for the depth-longitude cross-section of the correlation between ECPM and JPL equatorial DJF temperature anomalies. Contour interval 0.1. Correlations coefficients that are less than 95% significance level cutoff are masked